catalysts

MDPI

Article

Ring-Opening Polymerization of *rac*-Lactide Catalyzed by Octahedral Nickel Carboxylate Complexes

Alexey Nikiforov [1], Natalia Panina [2], Daniil Blinou [3], Vladislav Gurzhiy [4], Juliya Nashchekina [5], Evgenia Korzhikova-Vlakh [1,4,*], Alexey Eremin [1] and Mariia Stepanova [1,*]

[1] Institute of Macromolecular Compounds, Russian Academy of Sciences, St. Petersburg 199004, Russia
[2] Department of Inorganic Chemistry, Saint-Petersburg State Institute of Technology (Technical University), St. Petersburg 190013, Russia
[3] Kurnakov Institute of General and Inorganic Chemistry, Russian Academy of Sciences, Moscow 119991, Russia
[4] Saint-Petersburg State University, St. Petersburg 199034, Russia
[5] Institute of Cytology, Russian Academy of Sciences, St. Petersburg 194064, Russia
* Correspondence: vlakh@hq.macro.ru (E.K.-V.); maristepanova@hq.macro.ru (M.S.)

Abstract: To date, nickel(II) complexes have not been practically investigated as catalysts in ring-opening polymerization (ROP) of lactide to produce biodegradable poly(lactic acid), which is in demand in biomedicine and industry. In this study, carboxylate complexes of nickel(II) containing various N-donor ligands with different nuclearity, metal core rigidity and nature of carboxylate ligands were synthesized and studied by infrared spectroscopy, X-ray diffraction, elemental and thermogravimetric analyses. The obtained complexes were examined in the (ROP of the *rac*-lactide in bulk and in toluene solution with and without the addition of a benzyl alcohol initiator. In the series of complexes studied, the complex $[Ni(DBED)_2(O_2CC(CH_3)_3)_2]\cdot(CH_3)_3CCO_2H$ (DBED is *N*,*N*′-dibenzylethylenediamine) was a syndioselective catalyst and showed the highest catalytic ability in the polymerization without the addition of benzyl alcohol. For this complex, according to 1D DOSY ^{1}H NMR spectroscopy and mass spectrometry with electrospray ionization, polymerization is initiated by a free secondary amine, DBED, leaving the metal's inner coordination sphere. Based on the experimental data obtained, a comprehensive density functional theory (DFT) study of the ROP pathways including the initiation and first chain growth cycle steps with a detailed description of the intermediates and evaluation of the energy barriers of the steps was carried out. It was shown that one of the key roles in the reaction process is played by carboxylate ligands, which act as proton carriers from the initiator molecule and have a significant influence on the reactivity of the catalytic metal complexes.

Keywords: lactide; nickel; carboxylate ligands; molecular structures; mass-spectrometry; homogeneous catalysis; ring-opening polymerization; polylactide; DFT quantum-chemical modeling

Citation: Nikiforov, A.; Panina, N.; Blinou, D.; Gurzhiy, V.; Nashchekina, J.; Korzhikova-Vlakh, E.; Eremin, A.; Stepanova, M. Ring-Opening Polymerization of *rac*-Lactide Catalyzed by Octahedral Nickel Carboxylate Complexes. *Catalysts* **2023**, *13*, 304. https://doi.org/10.3390/catal13020304

Academic Editor: Adriana Maria da Silva

Received: 29 December 2022
Revised: 24 January 2023
Accepted: 26 January 2023
Published: 29 January 2023

1. Introduction

Poly(lactic acid) (or polylactide, PLA), which belongs to the class of aliphatic polyesters, is of great interest both for biomedical purposes and the manufacturing of various biodegradable consumer products and packaging materials [1–10]. Such interest is caused by the combination of biodegradability, biocompatibility, and the possibility to vary the mechanical properties of the materials made of this polymer. In addition, PLA is a thermoplastic polymer and is promising for replacing non-degradable petroleum-based plastics such as poly(ethylene terephthalate) and polystyrene [11–13]. Polylactide can be synthesized by direct polycondensation of lactic acid, but the optimal approach is catalytic ring opening polymerization (ROP) of lactide [14,15]. The most effective catalysts for ROP

are such homoleptic complexes as tin(II) octoate (2-ethylhexanoate) and aluminum(III) triisopropoxide [16–18]; however, only tin(II) octoate found industrial applications. Though this compound has undoubted advantages, it also has a number of significant drawbacks: complicated control over the PLA molecular weight characteristics, cytotoxicity [19,20], and difficulty of removal from the polymer mass. All of these factors can affect the engraftment and the environment negatively when using biomaterials and various products based on such PLA. Therefore, the development of biocompatible catalysts that allow obtaining PLA with high yield, different molecular weights and low cost is one of the priority tasks of both material science and fundamental chemistry.

A large number of different metal complex and organic catalysts have been studied [15,21–35], but organocatalysts seem to be more promising due to the absence of metals in their composition. However, the development of effective organocatalysts is still in progress, since the application of the most promising of them for ROP in bulk is limited by the following disadvantages: catalysis of transesterification and racemization of the polymer, low thermal stability or lower activity compared to metal-containing catalysts [22]. A large number of coordination and organometallic compounds of transition, alkali and alkaline earth metals have been investigated in the ROP of lactide [32,33,36–39]. Among them, compounds of magnesium [40] and calcium [41], which are biocompatible and have less toxicity in comparison with transition metal compounds, are especially noteworthy. However, their industrial application for PLA production is limited because of the instability of the complexes containing metals of group 2A (IIA) in the air or in the presence of moisture. Various studies have indicated the influence of the substituents in the ligands [42], the nuclearity of the catalyst [39,43], and the solvent and the kind of the metal used [44,45] on their reactivity. In most cases, this is due to the fact that the catalytic ROP reaction of lactide occurs by the coordination-insertion mechanism in which the initial formation of the active metal complex with the initiator molecule is followed by its insertion into the lactide structure with ring opening [46,47].

It is known that nickel(II) complexes have demonstrated great potential for applications as catalysts in synthetic organic chemistry [48–53]. Furthermore, since nickel is found in the composition of metal hydrolase enzymes, nickel(II) coordination compounds have been studied as models of the active centers of such enzymes [54]. There are a few publications reporting that nickel(II) complexes are active in the ROP of lactide [55–58]. In particular, nickel complexes with Salen-type Schiff-base ligands were synthesized and characterized by square planar geometry for the Ni atom [55–58], and the supposed mechanism of polymerization in the presence of benzyl alcohol as an initiator was presented [55]. However, only one study has reported the catalytic activity of nickel(II) compounds in solution [55] which is probably due to the poor solubility of the complexes in the most suitable solvents to ensure the homogeneous polymerization of lactide. Thus, the influence of the structure of coordination compounds on the ROP of lactide as well as the mechanism of the reaction catalyzed by nickel(II) compounds practically have not been studied.

In this study, the air-stable and organic solvents soluble octahedral mononuclear and binuclear mixed-ligand carboxylate nickel(II) complexes containing various N-donor and carboxylate ligands were synthesized using a simple synthetic route and carefully characterized. The catalytic ability of the complexes prepared was investigated in the ROP of *rac*-lactide (*rac*-LA) both in bulk and in solution with and without the addition of an initiator to the system. Finally, a mechanism of the ROP of *rac*-LA catalyzed by the mononuclear complex, which demonstrated the best catalytic properties, was assumed based on the results of spectral analysis and quantum-chemical modeling.

2. Results and Discussion

2.1. Synthesis and Structure Characterization of Ni Complexes

In order to study the mixed-ligand nickel(II) carboxylate complexes with ethylenediamine derivatives as catalysts in ring-opening polymerization (ROP) of cyclic esters (primarily for *D,L*-lactide), two mononuclear complexes with trans-configuration and two binuclear aqua-bridged complexes containing different carboxylate ligands in their nature were obtained. The selection of N-donor ligands was conditioned by the requirement of solubility of the catalytically active complexes under study in the lactide bulk and nonpolar organic solvents used for ROP. Another reason was a choice of drastically different steric factors and the nature of the amino group determining the formation of only mononuclear complexes in the case of *N,N′*-dibenzylethylenediamine (DBED) and binuclear complexes with *N,N,N′,N′*-tetramethylethylenediamine (TEMED).

Mononuclear *trans*-[Ni(DBED)$_2$(O$_2$CCF$_3$)$_2$]·C$_6$H$_6$ (**1**), *trans*-[Ni(DBED)$_2$(O$_2$CC(CH$_3$)$_3$)$_2$]·(CH$_3$)$_3$CCO$_2$H (**2**) and binuclear [Ni$_2$(μ-OH$_2$)(μ-O$_2$CCF$_3$)$_2$(O$_2$CCF$_3$)$_2$(TEMED)$_2$] (**3**) complexes were synthesized by reacting the appropriate nickel(II) carboxylates with the N-donor ligands DBED and TEMED. [Ni$_2$(μ-OH$_2$)(μ-O$_2$CC$_6$H$_5$)$_2$(O$_2$CC$_6$H$_5$)$_2$(TEMED)$_2$] (**4**) was obtained by the "one pot" technique via the sequential reaction of synthetic Hellyerite (NiCO$_3$·5.5H$_2$O) [59] with benzoic acid and TEMED in acetonitrile solution. The synthesis of all complexes did not require special conditions and they were stable in air. The general scheme for obtaining **1**–**4** is presented in Figure 1. A detailed description of the synthetic procedures can be found in Section 3.3.

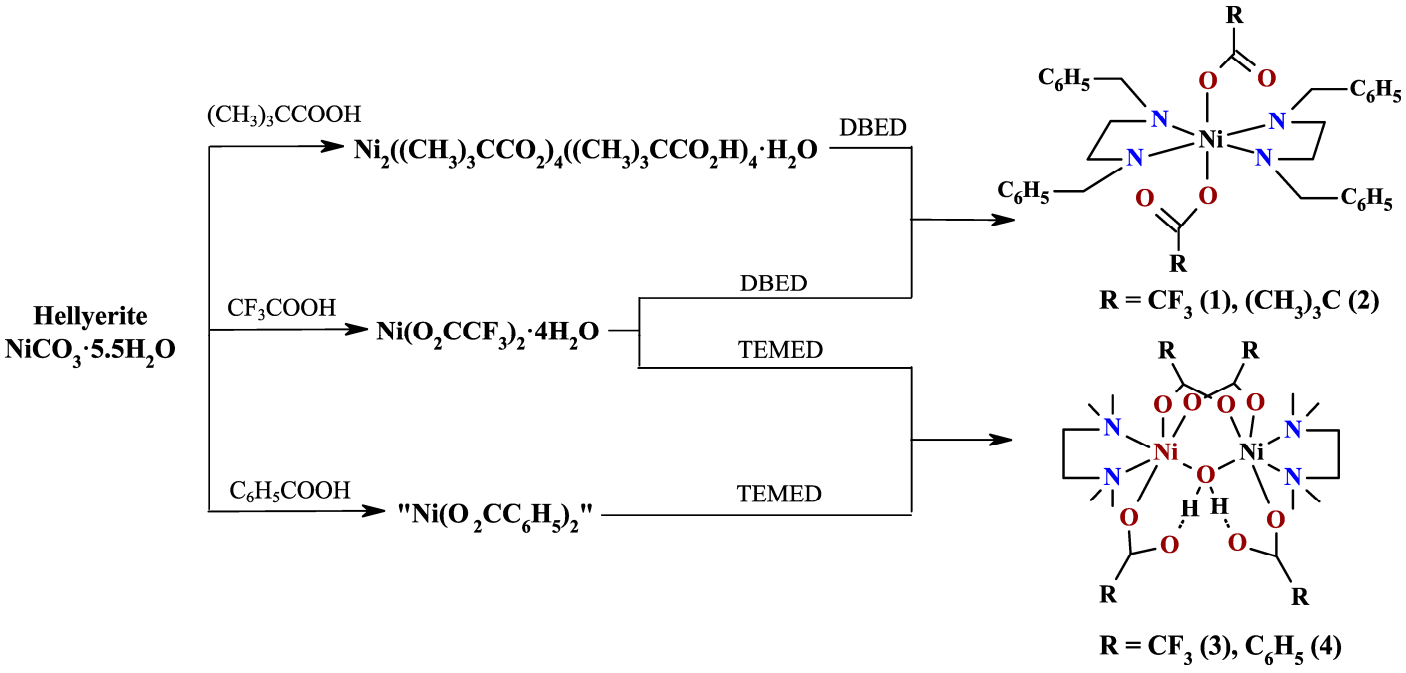

Figure 1. Synthetic routes of compounds **1**–**4**.

Complexes **1**, **2**, and **4** were synthesized for the first time. It should be noted that **4** was synthesized similarly to the procedure published for the preparation of [Ni$_2$(μ-OH$_2$)(μ-O$_2$CCH(CH$_3$)$_2$)$_2$L$_{2\text{-}4}$((CH$_3$)$_2$CHCO$_2$)$_2$] (L—various N-donor ligands) [60]. Complex **3** is known and was prepared according to previously reported procedures [61]. The monocrystals of the complexes were obtained by slow concentration in the air from solutions: benzene/methanol (r.t.) (**1**), tetrahydrofurane/n-hexane (ref.) (**2**), ethanol (r.t.) (**3**), and acetonitrile/water (r.t.) (**4**). Complexes **1** and **2** crystallize in the space groups *P*-1 (triclinic) and *P*2$_1$/*n* (monoclinic), respectively. Nickel atoms in the molecular structures of these compounds have a distorted *trans*-NiN$_4$O$_2$ octahedral environment formed by four nitrogen atoms of two bidentate-coordinated DBED-k^{2}N,N′ and two oxygen atoms of two O$_2$CR-kO (R = CF$_3$ (**1**) and C(CH$_3$)$_3$ (**2**))

occupying axial positions (Figure 2). In **1**, each of the carboxylate ligands forms one intramolecular hydrogen bond with one of the NH groups of the DBED ligand (d(N2···O2) = 2.893 Å). In **2**, the pivalic ligands form two hydrogen bonds with each NH group of the corresponding DBED ligands. The geometrical parameters of the intramolecular H-bonds **1** and **2** are summarized in Table S1 of Supplementary Materials.

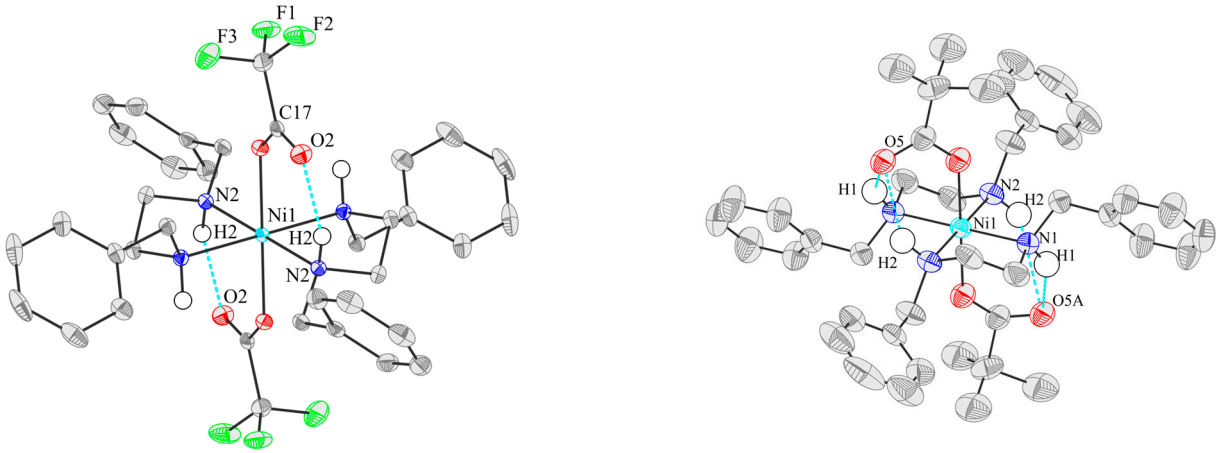

Figure 2. Molecular structures of **1** (**a**) and **2** (**b**) compounds (50% probability thermal ellipsoids). Dashed lines show intramolecular hydrogen bonds. H-atoms of DBED and pivalate ligand are omitted for clarity.

In the crystal structure of compound **1**, the molecules of the complex are connected into a polymer chain along the crystallographic axis [1 0 0] by two pairs of symmetric weak hydrogen bonds, C-H···F and N-H···F (Figure S1, Supplementary Materials). The emerging chains are combined into a three-dimensional supramolecular system due to weak C-H···O hydrogen bonds, as well as C-H···π interactions of the edge-to-face type involving phenyl fragments of DBED ligands. In addition, the molecules of the complex in the crystal are joined together by weak C-H···O hydrogen bonds with solvate benzene molecules along the crystallographic axis [1 0 1], with average C···O distances of 3.359 Å (See Figure S2, Supplementary Materials). According to the Hirschfeld surface (HS) analysis, the contributions of the observed interactions F···H, as well as H···O, H···H, C···H, and F···C in HS (Figure S3, Supplementary Materials) were 25.4, 4.1, 42.5, 24.2 and 1.7%, respectively.

Complexes **3** and **4** crystallize in the space groups $P2_1/n$ (monoclinic) [61] and P-1 (triclinic), respectively. The nickel atoms in **3** and **4** have a distorted NiN_2O_4 octahedral environment formed by nitrogen atoms of bidentate coordinated TEMED-k^2N,N′ and oxygen atoms of two μ-O_2CR-k^2O,O′, one μ-OH_2, and two O_2CR-kO. Two nickel ions are connected by bridging water molecules and two bridging carboxylate ligands O_2CR (R = CF_3 (**3**) and C_6H_5 (**4**)). The coordination environment of each nickel ion in both cases is complemented by one bidentate-coordinated TEMED ligand and one monodentate-coordinated carboxylate O_2CR ligand. The monodentate coordinated carboxylate ligands of **3** and **4** form an intramolecular hydrogen bond with the bridged water molecule. Figure 3 shows the molecular structure of complex **4**.

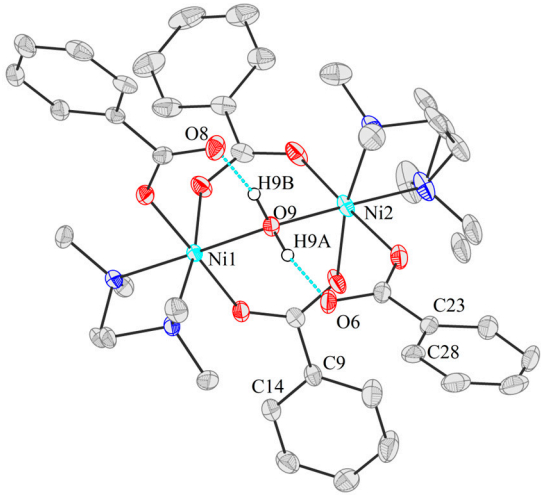

Figure 3. Molecular structures of compound **4** (50% probability thermal ellipsoids). Dashed lines show intramolecular hydrogen bonds. H-atoms of TEMED and benzoate ligand are ommited for clarity.

Binuclear aqua-bridged nickel(II) carboxylates possessing a similar structural motif are known [62–65] and were previously investigated as models of active centers of metal-containing hydrolases [54] and systems with interesting magnetic properties [66]. For compounds **3** and **4**, the values of the main bond lengths and valence angles are close to those in complexes with a similar core [60]. In the crystal structure of compound **4**, the subunits of the binuclear complexes are connected by two offset face-to-face π···π-stacking interactions (C23–C28···C23–C28 and C9–C14···C9–C14 atoms of C_6H_5 rings) with the formation of a zig-zag ensemble in the crystallographic axis [1 1 0] (Figure S4, Supplementary Materials). The distances between the symmetry centers of the phenyl substituents of the benzoate ligands in this interaction are Cg1···plane—3.421Å (Cg1 is the centroid of the C23-C28 C_6H_5 ring) and Cg2···plane—3.533Å (Cg2 is the centroid of the C9-C14 C_6H_5 ring), which is typical for this type of interaction [67,68]. Molecules **4** connect along the crystallographic axis [0 1 0] by C-H···π edge-to-face interactions of phenyl substituent of benzoate ligands (Figure S5, Supplementary Materials). The average C-H-plane distance of the aromatic system is 2.67 Å. The most intense bright red areas on the HS correspond to the C-H···π and C-H···O contact pairs (Figure S6a, Supplementary Materials). The C···C contact zones of π-stacking interactions on the HS over the shape index maps are areas with blue and red triangles united along a common vertex (Figure S6b, Supplementary materials). The contributions of H···H, C···H, C···C, and H···O contacts to the HS are 69.2, 26.1, 1.7, and 3.0%, respectively. The values of the average bond lengths Ni-N (DBED, TEMED) and Ni-O (O_2CR, OH_2) of the metal cores **1**–**4** are presented in Table S2 (Supplementary Materials).

The study of the reaction of *rac*-LA polymerization in the presence of the complexes involves the application of elevated temperatures. The thermal stability of **1**–**4** was investigated by thermogravimetric analysis (TGA). According to the TGA data, compound **1** lost the benzene solvate molecules in a sufficiently wide temperature range ~(70–145) °C (Figure S7, Supplementary Materials). The following stage of mass loss began at 180 °C. The thermal decomposition of **1** was completed at 470 °C with the formation of NiO mainly (Δm_{exp} = 92.28%, Δm_{calc} = 91.90%). In case of **2**, the loss of pivalic acid solvate molecules also started at ~70 °C and was completed at 145 °C. Then, there was a thermal decomposition of the complex continuing up to 450 °C (Figure S8 of Supplementary Materials). It is known that the thermal stability of binuclear aqua-bridged nickel(II) carboxylates with bidentate N-donor ligands in the temperature range up to PLA melting point (up to 140–150 °C) depends slightly on the carboxylate substituent and, in general, such compounds exhibit similar thermal behavior to each other [60,65,69]. To further confirm the stability of the complexes in model polymerization reactions, the thermal behavior of

bidentate aqua-bridged mixed-ligand nickel(II) carboxylates was investigated using example **4** (Figure S9, Supplementary Materials). Complex **4** was stable up to 150 °C; further heating in the temperature range of 152–249 °C resulted in a loss of 10.88% of mass with a negligible endothermic effect. The second stage of thermodestruction was characterized by a decomposition initiation temperature of 252 °C and continued up to 387 °C, accompanied by a high rate of loss of 72.14% of the mass. Thus, all compounds are not decomposed up to 145 °C, which indicates their applicability for both *rac*-LA polymerization in bulk and in solution under heating.

2.2. Ring-Opening Polymerization of rac-Lactide

The influence of the reactivity of mixed-ligand nickel(II) carboxylate complexes of different nuclearity, metal core rigidity, and nature of ligands as catalysts was investigated in the *rac*-lactide ROP. It was assumed that polymerization should have proceeded along the path of primary coordination of the monomer to the complex and the subsequent growth of the polymer chain for both the studied mononuclear (**1** and **2**) and binuclear (**3** and **4**) complexes. All complexes are characterized by similar structural parameters but differ in the structure of the metal core, the geometric environment of the metal ion, and the steric factors of N-donor and electron-withdrawing carboxylate ligands. Taking into account the occupancy of the nickel coordination sphere of complexes **1–4**, it can be assumed that the binding of the monomer molecule to the metal center can occur via the S_N1 substitution mechanism or after leaving the N-donor ligand from the inner sphere of the complex as a result of its dissociation [70]. From this point of view, binuclear complexes (**3** and **4**) with a kinetically inert metal core should exhibit a lower relative catalytic ability. Additionally, the presence in **1–4** of carboxylate ligands, which differ greatly in basicity, will allow a determination of their role (as proton carriers) in the ROP of *rac*-LA. To support the assumptions made, all complexes were tested for their ability to act as *rac*-lactide ROP catalysts. The reactions were carried out in solution (toluene) and in bulk with monomer to complex (designated as [Ni]) ratios of 250/1 and 500/1 at 140 °C under Ar for 72 h in the presence and without an initiator (benzyl alcohol, BnOH). The resulting PLA samples were analyzed by size-exclusion chromatography (SEC). The molecular-weight characteristics and conversion of the monomer are presented in Table 1. In addition, the catalyst turnover number (TON, mol of converted monomer/mol of catalyst) and the turnover frequency (TOF, TON/reaction time) were calculated as described elsewhere [71].

Table 1. ROP of *rac*-lactide catalyzed by the Ni complexes **1–4**.

Catalyst	[*rac*-LA]/[Ni]/[BnOH]	In Toluene				In Bulk			
		M_n	$Đ$	Conv. (%)	TON	M_n	$Đ$	Conv. (%)	TON
1	250/1/0	5400	1.4	45	112	6300	1.4	84	210
	250/1/1	5800	1.5	58	145		n/d		
	500/1/0	600	1.1	6	30	7400	1.5	52	260
2	250/1/0	5800	1.5	69	172	7500	1.7	98	245
	250/1/1	6000	1.6	78	195		n/d		
	500/1/0	6300	1.4	31	155	9000	1.6	84	420
3	250/1/0	1400	1.0	<1	-	1300	1.0	<1	-
	250/1/1	800	1.0	<1	-		n/d		
	500/1/0	800	1.0	<1	-	800	1.0	<1	-
4	250/1/0	2700	1.5	58	145 *	3700	1.1	21	52 *
	250/1/1	2000	1.3	79	197 *		n/d		
	500/1/0	2500	1.3	25	125 *	1900	1.1	8	40 *

Reaction conditions: *rac*-LA 3.5 mmol, toluene 0 or 2 mL, Ar atmosphere, 140 °C, 72 h. Monomer conversion, dispersity ($Đ$) and number average molecular weight (M_n) were determined by SEC of the crude reaction mixture (tetrahydrofurane, polystyrene calibration standards, 40 °C); [Ni]—

amount of complex; n/d—not determined; the TON was determined from the ratio of moles of converted monomer to moles of catalyst. * Determined based on the fact that the catalyst was a binuclear complex.

It was noted that the polymerization reaction proceeded regardless of the presence or absence of BnOH. The introduction of one molar equivalent of BnOH relative to the nickel complexes into the reaction mixture had almost no effect on the M_n of the resulting PLA but led to some increase in monomer conversions and the TON of catalysts. In addition, all the studied complexes, with the exception of **3**, showed the ability to catalyze the reaction both in solution and in bulk. The established TOF values for **1**, **2** and **4** were predominantly 2–3 h^{-1}. An analysis of the molecular weights of the obtained PLA samples showed that the highest and closest values of M_n (5400–7500) were obtained using mononuclear complexes **1** and **2**, mainly at a [*rac*-LA]/[Ni] ratio of 250/1. The highest conversion and TON values were also observed for the same catalytic systems; however, in the case of complex **2**, these parameters were higher by ~30% compared to **1** and amounted to ≥69% and 172, respectively. Increasing the [*rac*-LA]/[Ni] ratio up to 500/1 for **1**–**4** resulted in a decrease in conversion, and the highest M_n was obtained using **2**. As expected, binuclear complex **4** exhibited significantly lower catalytic properties compared to mononuclear compounds (low values of M_n, conversion and TON), while for **3** it was practically absent. Thus, such a behavior of the studied binuclear compounds could be associated with a significantly higher stability of the binuclear metal core under the reaction conditions and low availability of the metal center for monomer coordination. In the case of **3**, this can be exacerbated by the possibility of electrostatic repulsion between the monomer molecule and the trifluoromethyl groups of the carboxylate ligands. In accordance with known mechanisms of coordination-insertion using metal carboxylates (for example, tin(II) octoate [72]), a proton is transferred from the initiator molecule to the carboxylate ligand during the reaction. Equilibrium proton transfer to $CF_3CO_2^-$ is less probable compared to anions of pivalic or benzoic acids ($pK_a(CF_3CO_2H)$ ~0.2, $pK_a((CH_3)_3CCO_2H)$ ~5), which may additionally explain the lower catalytic activity of **1** and **3**. However, protonation of the terminal alkoxide group of the growing polymer chain by the formed carboxylic acid is possible and, in turn, can lead to chain termination. It is also likely that the described processes are realized simultaneously. Thus, the use of mononuclear mixed-ligand nickel(II) carboxylates containing RCO_2 ligands with high basicity and labile N-donor ligands as catalysts in *rac*-LA ROP seems to be the most promising.

In this regard, further studies of the effect of temperature and time of the polymerization on monomer conversions and PLA molecular weights were investigated using pivalate complex **2** (Table 2). The reactions were carried out in a toluene solution of *rac*-lactide at a ratio of [*rac*-LA]/[Ni] = 250/1, varying the polymerization temperature and time in the ranges of 100–140 °C and 24–72 h, respectively.

Table 2. ROP of *rac*-LA in toluene catalyzed by complex **2** under different conditions.

Entry	Temp. (°C)	Time (h)	M_n *	$Đ$ *	Conv. * (%)
1	140	72	5800	1.5	69
2	130	72	4400	1.6	68
3	120	72	3000	1.3	46
4	110	72	3000	1.3	51
5	100	72	2700	1.2	34
6	100	48	2600	1.2	31
7	100	24	900	1.1	19

Reaction conditions: *rac*-LA 3.5 mmol, [*rac*-LA]/[Ni]—250/1, toluene 2 mL, Ar atmosphere. * Determined by SEC of the crude reaction mixture (tetrahydrofurane, polystyrene calibration standards, 40 °C).

Achieving a monomer conversion of more than 50% was possible at temperatures above 130 °C for 72 h. A further increase in temperature (up to 140 °C) did not affect the conversion but led to an increase in M_n. Thus, a more detailed study of the dependence of monomer conversions and M_n values of PLA on polymerization time was carried out at a temperature of 140 °C. The resulting dependencies are shown in Figure 4.

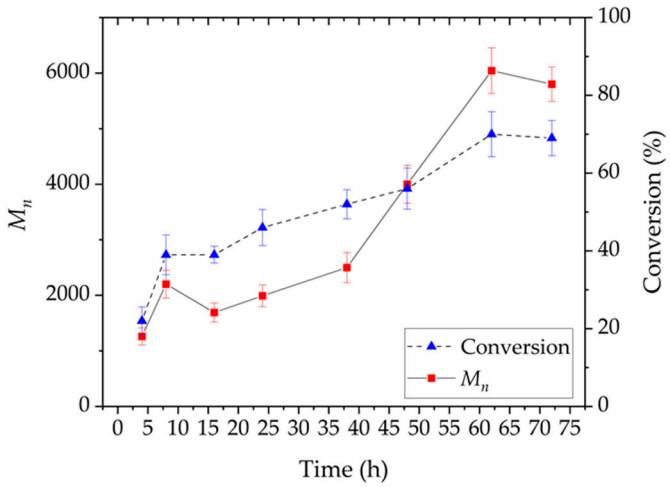

Figure 4. M_n and monomer conversion as functions of reaction time in the polymerization of *rac*-lactide with complex **2**. Conditions: *rac*-LA 3.5 mmol, [*rac*-LA]/[Ni]—250/1, toluene 2 mL, 140 °C, Ar atmosphere. The values were determined by SEC (tetrahydrofurane, polystyrene calibration standards, 40 °C) of the crude reaction mixture.

The observed almost complete absence of changes in M_n values from ~8 to 38 h of polymerization, accompanied by a slight increase in the conversion of the monomer, may be related both to the onset of intramolecular catalytic esterification [73,74] of the resulting PLA, and to a significant rearrangement of the catalytic complex structure followed by a change in the catalytic properties (a sharp increase in these parameters).

For catalyst **2**, its stereoselectivity was determined by analyzing the carbonyl region of the ^{13}C NMR spectrum of PLA as described in [75]. The stereoselectivity coefficient P_i for PLA obtained in a toluene solution; the ratio [*rac*-LA]/[Ni]/[BnOH] = 250/1/0 was 0.33. PLA synthesized under analogous conditions using complex **1** was characterized by a close value of this coefficient (P_i = 0.36). An example of the corresponding fragment of the ^{13}C NMR spectrum of PLA is shown in Figure S10 (Supplementary Materials). Such values of the P_i coefficients (<0.5) indicate a predominantly syndiotactic polymerization process.

2.3. Mechanistic Aspects of Polymerization

2.3.1. Spectroscopy Investigation

High-resolution electrospray ionization (ESI) mass spectrometry was used to identify moieties present in reaction mixtures of polymerization systems in order to determine the polymerization pathway of *rac*-lactide. For this analysis, model systems containing *rac*-LA oligomers obtained by polymerization in a toluene solution (72 h, 140 °C, argon atmosphere) with molar ratios *rac*-LA/complex **2** equal to 2/1 and 3/1 were used.

In the ESI mass-spectra of acetonitrile solutions from both model polymerization mixtures, a number of signals assigned to ions of the composition ((DBED)(Lac)$_n$) + Na$^+$ (n = 2–10, Lac is lactoyl OCH$_3$CHCO group) were detected. In addition, a series of signals with a mass-to-charge ratio (*m*/*z*) shift of 12.036 was observed in the obtained mass spectra. Such a shift may correspond to the formation of ions of composition ((DBED)(Lac)$_n$ + C_2H_4–O) + Na$^+$ (n = 2–10) [76], which can genetically originate from catalytically degraded lactoyl units. The correlated signals in the received mass-spectra, theoretically calculated

and experimentally obtained *m*/*z* values are summarized in Table 3. It can be assumed that the free DBED ligand leaving the inner sphere of the complex was the moiety initiating the ring-opening polymerization of the lactide. The ROP of lactide initiated by secondary amines is known [77–80]. To confirm the possibility of the appearance of such initiating units in the system for the studied mononuclear complexes, an ESI mass spectrometric study was performed. The resulting ESI mass-spectrum of an acetonitrile solution of compound **2** contained an intense signal corresponding to the protonated ligand $(DBED+H)^+$ (*m*/*z* = 241.170). Intense signals corresponding to the fragment $[Ni(O_2CC(CH_3)_3)(DBED)_2]^+$ (*m*/*z* = 639.320) and ion $[Ni(O_2CC(CH_3)_3)(DBED)]^+$ (*m*/*z* = 399.157) have also been observed. The results of the comparative analysis of a solution of complex **1** showed similar behavior to this compound. This is confirmed by the presence in the ESI mass-spectrum of signals from the protonated ligand $(DBED+H)^+$ (*m*/*z* = 241.170) and singly charged ions similar to complex **2** ($[Ni(O_2CCF_3)(DBED)_2]^+$—*m*/*z* = 651.247, $[Ni(O_2CCF_3)(DBED)]^+$—*m*/*z* = 411.084, $[Ni_2(O_2CCF_3)_3(DBED)_2]^+$—*m*/*z* = 935.150 and cationized molecule $[Ni(O_2CCF_3)_2(DBED)_2+H]^+$—*m*/*z* = 765.237).

Table 3. Calculated molecular formulas and masses of dialkyl lactamide species in ESI mass-spectra of model polymerization mixture.

n	$((DBED)(Lac)_n) + Na^+$		$((DBED)(Lac)_n + C_2H_4{-}O) + Na^+$	
	$m/z_{(experimental)}$	$m/z_{(theoretical)}$	$m/z_{(experimental)}$	$m/z_{(theoretical)}$
2	407.1953	407.1947	not detected	347.2099
3	479.2165	479.2158	491.2544	491.2522
4	551.2378	551.2369	563.2333	563.2733
5	623.2591	623.2581	635.2955	635.2944
6	695.2804	695.2792	707.3168	707.3156
7	767.3016	767.3003	779.3382	779.3367
8	839.3230	839.3214	851.3594	851.3578
9	911.3444	911.3426	923.3806	923.3789
10	983.3666	983.3637	995.4020	995.4001

Oligomerization conditions: [*rac*-LA]/[Ni] 3/1, toluene, 140 °C, 72 h, Ar atmosphere.

The ESI mass-spectra of complexes **1** and **2** exhibited a number of signals corresponding to the formate complexes $[Ni(O_2CH)(DBED)_2]^+$ (*m*/*z* = 583.257), $[Ni_2(O_2CH)(O_2CC(CH_3)_3)_2(DBED)_2]^+$ (*m*/*z* = 843.313) and conversion products of DBED ligands, namely, formylated DBED ($(DBED+CHO)^+$, m/z = 269.166) and *N*,*N*′-dibenzyldihydroimidazolium cation ($(C_{17}H_{19}N_2)^+$, *m*/*z* = 251.155). A number of adduct signals of the previously mentioned ions with the carbonyl fragment $((DBED)(Lac)_n(CO)) + Na^+$ (n = 1–9) and $(DBED)(Lac)_n(CO) + C_2H_4{-}O + Na^+$ (n = 1–9)) was also detected in the obtained mass-spectra of model polymerization systems. Such adducts may be formylated dialkyl lactamide derived from lactic acid oligomers or carboxylate ligands. The theoretical and experimental mass values associated with these signals can be found in Table S3 (Supplementary Materials). The origin of formylated products in the spectra can be explained by the presence of sodium formate in the system used to calibrate the instrument. The probable formation scheme of the $(DBED+CHO)^+$ and $(C_{17}H_{19}N_2)^+$ ions [81–83], as well as the proposed structure of the $[(DBED)(Lac)_n(CO)]$ adduct, are presented in Figure S11 (Supplementary Materials). The mass-spectra of complexes **1** and **2** and a model polymerization mixture using the [*rac*-LA]/[Ni] ratio of 3/1 are shown in Figures S12 and S13 (Supplementary Materials), respectively.

Thus, according to mass spectrometry data, nickel(II) mononuclear carboxylate complexes (**1**, **2**) in the solution are able to form the $[Ni(O_2CR)(DBED)_2]^+$ ion and, further, can lose one of the DBED ligands to form $[Ni(DBED)(O_2CR)]^+$.

The assumption about the role of DBED ligands as the initiator of the considered polymerization process was additionally confirmed by the results of NMR spectroscopy

of the studied polymers. The signals assigned to the hydrogen atoms of the DBED molecule were observed in both ^{1}H NMR and 1D DOSY (one-dimensional diffusion ordered spectroscopy) ^{1}H NMR spectra of the reprecipitated polymers obtained using compound **2** ([*rac*-LA/[Ni]] ratio of 250/1 and 500/1, polymerization in toluene, 72 h). ^{1}H NMR signals at 7.45–7.03 ppm were assigned to the aromatic protons of the phenyl substituents of the terminal DBED. The multiplet at 4.36 and 2.74 ppm corresponded to the CH protons of the polylactide chain terminal unit and to the terminal OH group [84], respectively. The ^{1}H NMR spectrum of the reprecipitated polylactide obtained in a toluene solution using **2** at a ratio of [*rac*-LA]/[Ni] 500/1 is shown in Figure 5 as an example.

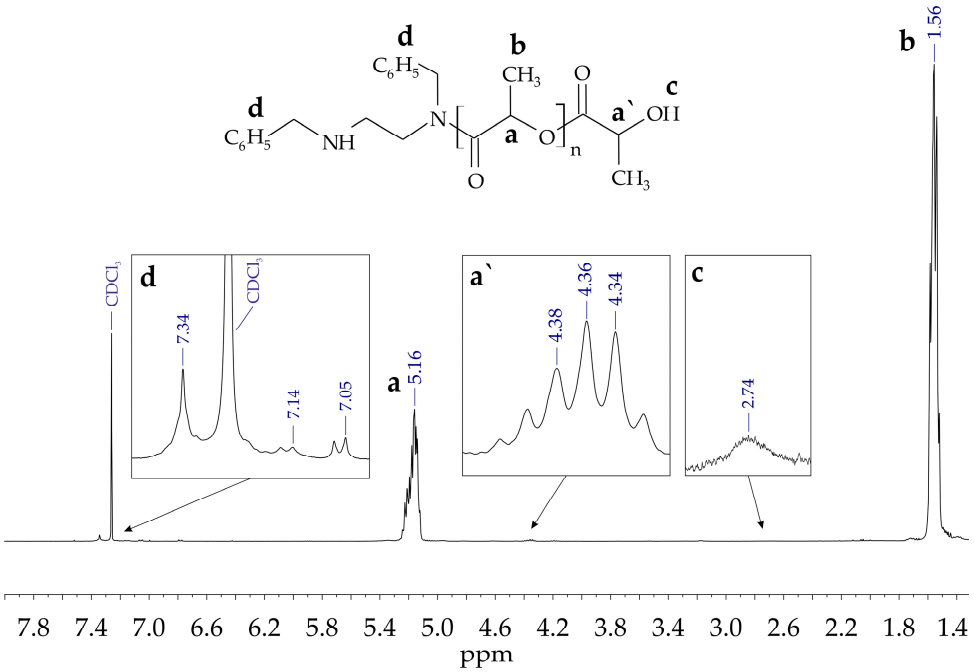

Figure 5. ^{1}H NMR spectrum in $CDCl_3$ of PLA, obtained using complex **2**. Polymerization conditions: [*rac*-LA]/[Ni] 500/1, toluene, 72 h, 140 °C.

The study performed using 1D DOSY ^{1}H NMR at a gradient intensity of 90% demonstrated the absence of the $CDCl_3$ signal in the obtained spectrum and the presence of PLA and DBED signals (Figure S14 of Supplementary Materials), which indicated that DBED was associated with the polymer chain.

Thus, the analysis by ESI mass spectrometry and ^{1}H NMR spectroscopy of PLA and lactide oligomers synthesized using complex **2** showed DBED and OH as end groups, which confirms that polymerization was initiated by secondary amine DBED leaving the inner coordination sphere **2**. The proposed reaction scheme and the structure of the polymer obtained upon initiation with the DBED amino group, and probably also valid for complex **1**, are shown in Figure 6.

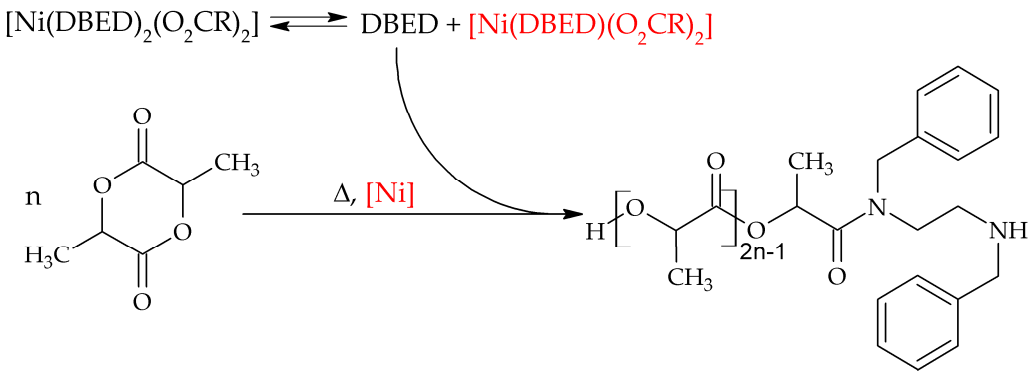

Figure 6. Graphical representation for ROP reaction of *rac*-LA initiated by DBED (R = CF_3, $C(CH_3)_3$).

2.3.2. Quantum-Chemical Modelling

In this study, it is assumed that the lactide (LA) ROP reaction in the presence of a nickel(II) mononuclear carboxylate complex (**1** or **2**) containing a coordinated secondary amine DBED and initiated by DBED molecules leaving the inner sphere of the complex is described by the coordination–insertion mechanism. In order to reduce the time of quantum-chemical calculations for complex **2**, a simplified model was used. Bulky pivalate ligands were replaced by acetate ions; secondary amine *N*,*N*′-dimethylethylenediamine (DMED) was used as the coordinated N-donor ligand, and dimethylamine (DMA) was used as the initiator. Thus, the model complex $[Ni(DMED)_2(O_2CCH_3)_2]$ was considered as a catalyst. Before quantum-chemical calculations of the initiation step were performed, two possible isomers of the initial model compound were modeled to determine the lower-energy structure and energy effect of ligand coordination. Thus, the initial model coordination compound $[Ni(DMED)(O_2CCH_3)_2]$ (**I**) with an N-donor ligand that has left the inner coordination sphere can have two isomers: with an octahedral environment of the metal ion with bidentate coordination of both carboxylate ligands (**Ia**) and square pyramidal in the case of monodentate coordination of one of the $O_2CCH_3^-$ (**Ib**) anions. The addition reactions of the LA molecule to complexes **Ia** and **Ib** lead to the formation of the compound $[Ni(DMED)(LA)(O_2CCH_3)_2]$ (**II**) (Figure 7).

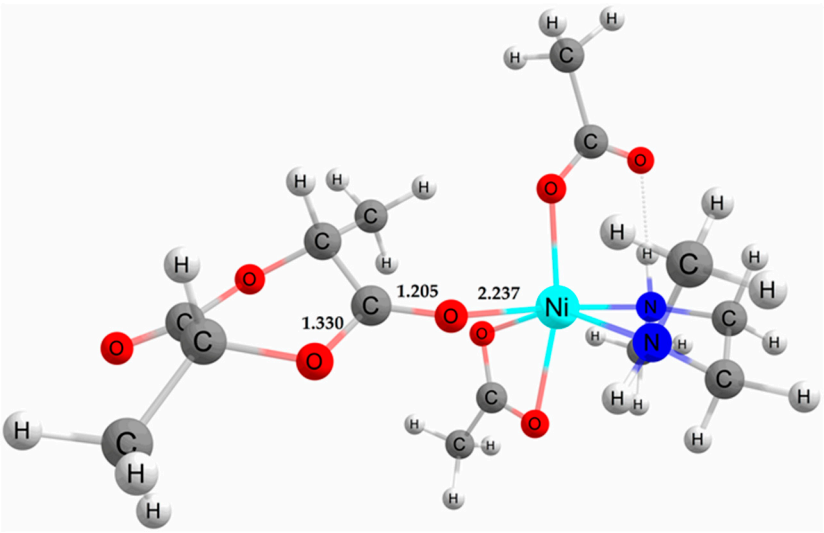

Figure 7. Optimized structure of the model compound $[Ni(DMED)(LA)(O_2CCH_3)_2]$ (**II**). Bond lengths are given in Å.

According to the data obtained, the energy effects of both reactions differ slightly from each other: ΔE+ZPE are −9.22 and −2.01 kcal/mol for **Ia** and **Ib**, respectively. In the optimized structure **II**, the environment of the nickel ion becomes octahedral, and the distance *d*(Ni-O1) is 2.237 Å (see atomic numbering in Figure 8). These values of bond lengths are typical for systems similar to structure **II** [85,86].

A schematic representation of the ROP reaction initiation step based on the calculations of the optimized structures is shown in Figure 8. Optimization of the possible reaction path was carried out taking into account approximately found transition states (TS) using the nudged elastic band with the TS optimization method (NEB-TS) [87] with the subsequent refinement of TS and intermediates along the reaction coordinate, which led to a decrease in the calculated activation barriers. The minimum energy path for **ESC→X** transitions is shown in Figure 9.

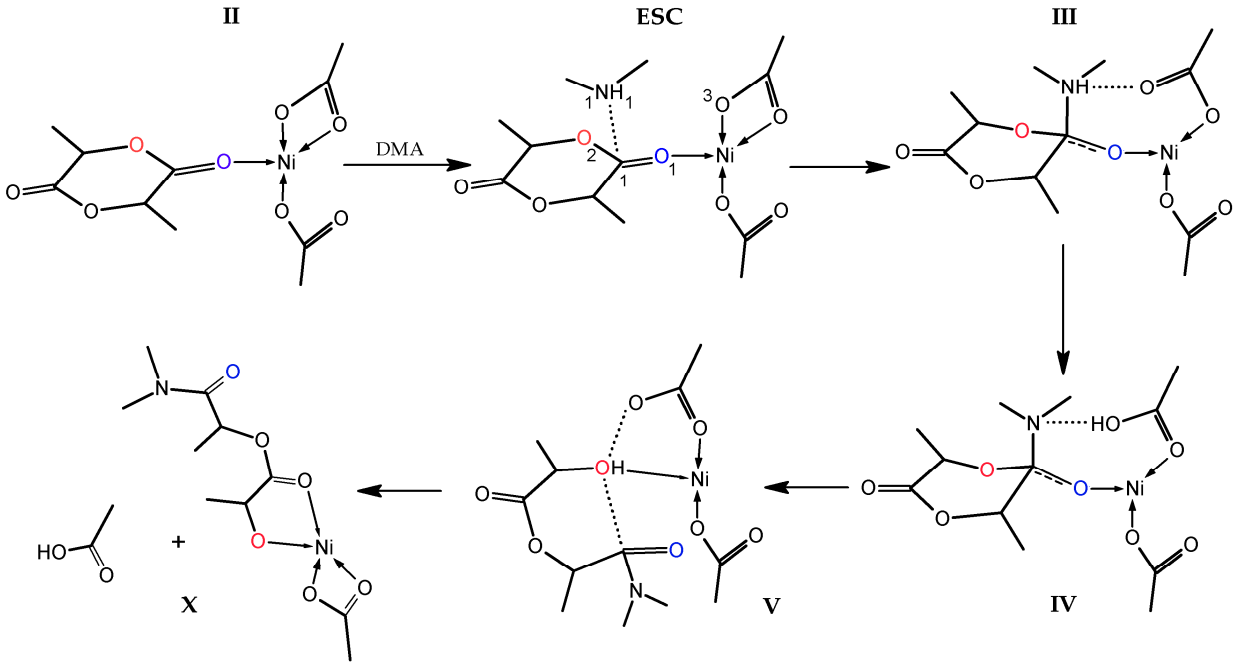

Figure 8. Proposed initiation step of LA coordination-insertion ROP mediated by model compound [Ni(DMED)$_2$(O$_2$CCH$_3$)$_2$] with optimized structures numeration. Coordinated DMED ligand are omitted for clarity. **ESC**—electrostatic complex.

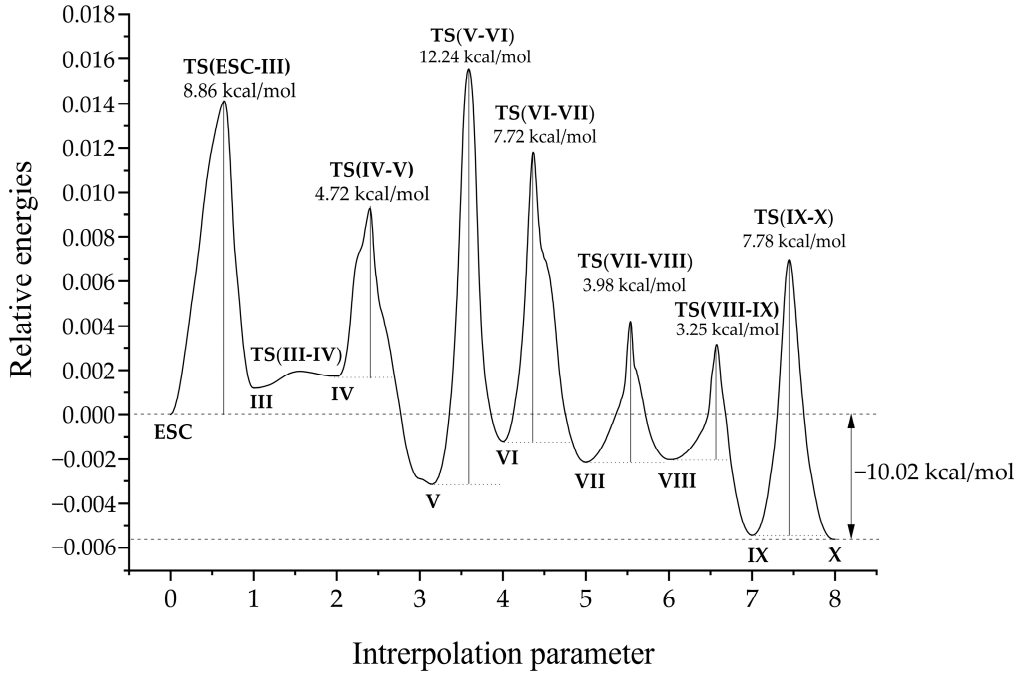

Figure 9. Minimum energy path between **ESC** and **X**.

The stage of initiation of the lactide ring-opening reaction is preceded by the formation of an electrostatic complex **ESC** with a secondary amine DMA molecule with a distance *d*(N1-C1) = 2.833 Å (Figure 10), which corresponds to a decrease in the energy of the system by −7.27 kcal/mol.

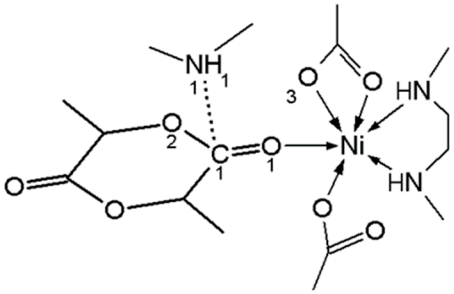

Figure 10. Schematic representation of the structure of **ESC** with atomic numbers.

The further approach of the DMA molecule, which may be the beginning of the nucleophilic attack of DMA on the carbonyl carbon atom of the lactide, leads to the formation of the transition state **TS(ESC-III)** (Figure 10). In the structure **TS(ESC-III)**, compared to ESC, the distance *d*(Ni-O1) decreases by 0.098 Å; the distance *d*(C1-O2) in the lactide ring increases by 0.075 Å. The NH group of DMA forms an intermolecular hydrogen bond with the carbonyl oxygen atom of the nearest carboxylate ligand. In this case, the coordination of the carboxylate ligand becomes monodentate, and the coordination environment of the central nickel ion becomes square-pyramidal. The activation energy of **TS(ESC-III)** equals 8.86 kcal/mol. This value is comparable to the activation barriers of similar reaction stages obtained previously for Al, Sn, and other metal complexes [88–90]. The formation of intermediate **III** corresponds to a further decrease in the distance *d*(N1···C1) to 1.547 Å and an increase in the bond lengths within the lactide ring to *d*(C1-O1) = 1.305 and *d*(C1-O2) = 1.424 Å. The carbonyl carbon atom in the LA molecule subjected to nucleophilic attack is in a nearly tetrahedral configuration (sp^3-hybridization). After the formation of intermediate **III**, the next step was the almost barrier-free transition of the H1 atom from the NH group of the DMA initiator to the O3 atom of the carboxylate ligand with the

formation of intermediate **IV**. In the optimized structure **IV**, at an N1–C1 distance of 1.500 Å, a covalent bond N1–C1 and a hydrogen bond N1–H1 are formed, while the bond lengths *d*(C1–O1) and *d*(C1–O2) increase to 1.323 and 1.433 Å, respectively.

Opening of the LA cycle occurs during the transition of structure **IV** to **V** with the overcoming of the transition state **TS(IV–V)**. The activation energy of this stage is 4.72 kcal/mol. In **TS(IV–V)**, the distance *d*(C1-O2) in the lactide cycle increases to 1.807 Å, and the O2 atom forms a hydrogen bond with the H1 atom, which originally belonged to DMA and then passed to the O atom of the carboxylic acid.

The following significant changes in the structure of **V** compared to **IV** should be noted: the breaking of the bonds between the Ni(II) ion and the lactide O1 atom (*d* = 3.674 Å) and the bond C1-O2 (*d* = 2.713 Å), as well as the formation of new bonds of the lactide O2 atom with the Ni and H1 atoms (*d*(O2-Ni) = 2.174 Å, *d*(O2-H1) = 1.068 Å). Subsequent local minima along the minimum energy path are associated with the formation of **VI–X** intermediates. Intermediate **VI** is formed from **V** with an activation barrier of 12.24 kcal/mol through the **TS (V–VI)** transition state. In the **TS(V–VI)** structure, the distance *d*(C1-O2) in the lactide cycle increases to 2.781 Å, and the H1 atom migrates from O2 to the oxygen atom of the carboxylic acid. The resulting acetic acid molecule begins to turn toward the second carboxylate ligand with the formation of a hydrogen bond with its O atom. In intermediate **VI**, the lactide ring opens up even more, *d*(C1-O2) = 2.996 Å. The subsequent formation of intermediate **VII** requires the transition of the energy barrier **TS(VI–VII)** equal to 7.72 kcal/mol. In the octahedral structure **VII**, one terminal fragment of lactic acid is bidentately coordinated to the Ni(II) ion, forming a five-membered ring with it, and the other is an *N*,*N*-dimethyllactamide group. The distance *d*(N1···C1) is 1.363 Å and is almost equal to the analogous distances in *N*,*N*-dimethylacetamide and *N*,*N*-dimethylformamide [91]. During the transition from intermediate **VII** to **VIII** and **IX**, the energy barriers in **TS(VII–VIII)** and **TS(VIII–IX)** with relatively low energies of 3.98 and 3.25 kcal/mol, respectively, are overcome. In intermediates **VIII** and **IX** of similar structure, one of the O_2CCH_3 anions retains monodentate coordination with the metal ion. Another similar anion, which added the H1 atom and turned into a coordinated acetic acid molecule during the formation of intermediate **VI**, is kept near the inner sphere of the metal ion only due to two hydrogen bonds. One of them is formed by the O atom of the acid and the H atom of the bidentately coordinated DMED ligand, the second is formed by its own H atom and the oxygen O2 of the lactide involved in the formation of the five-membered ring. As a result, the coordination environment of the central nickel ion again becomes square-pyramidal. In the subsequent intermediate **X**, the previous monodentately coordinated O_2CCH_3 ligand forms a second bond with Ni(II) and acquires bidentate coordination. As a result, the metal ion again acquires an octahedral environment, and the activation energy of this stage is 7.78 kcal/mol. The optimized structure of **X** is shown in Figure S15 (Supplementary Materials).

Further growth of the polymer chain requires the binding of another LA molecule to the metal ion and the opening of the LA ring by the coordination-insertion mechanism, in which the initiating group will be the terminal alkoxide group coordinated to the nickel(II) ion. Thus, when another LA molecule is coordinated to **X**, the type of coordination of the terminal unit of the oligomeric chain changes from bidentate to monodentate, followed by the formation of a stable structure **XI** (Figure S16 of Supplementary Materials). The simulated path of the first chain growth stage after passing through the initiation stage is shown in Figure 11.

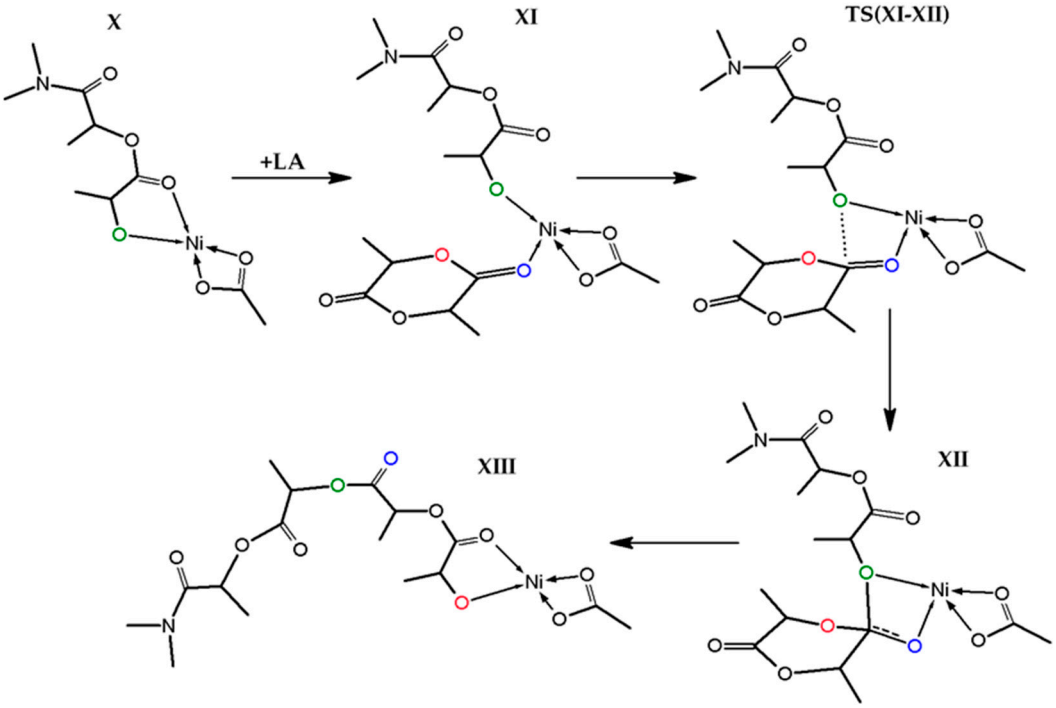

Figure 11. Proposed reaction path of the first propagation step. Coordinated DMED ligand are omitted for clarity.

A slight increase in the energy of the system during lactide coordination and the transition between **X**→**XI** (2.75 kcal/mol, see Figure 12) can be associated both with the steric features of the structure of **IX** and with a change in the type of coordination of the terminal unit of lactic acid from bidentate to monodentate. Further processes leading to the ring opening of the next coordinated monomer molecule are similar to those described above. These include nucleophilic attack of the terminal alkoxy group on the carbonyl carbon of the lactide to form intermediate **XII**, followed by direct ring opening of the lactide to form **XIII**, an optimized structure of which is shown in Figure S17 (Supplementary Materials). The energy change for the **XI**→**TS(XI–XII)**, **TS(XI–XII)**→**XII** and **XII**→**XIII** transitions is 2.23, 3.07 and 3.35 kcal/mol, respectively. In general, the energy profile of the stages of initiation and the first cycle of chain growth is presented in Figure 12.

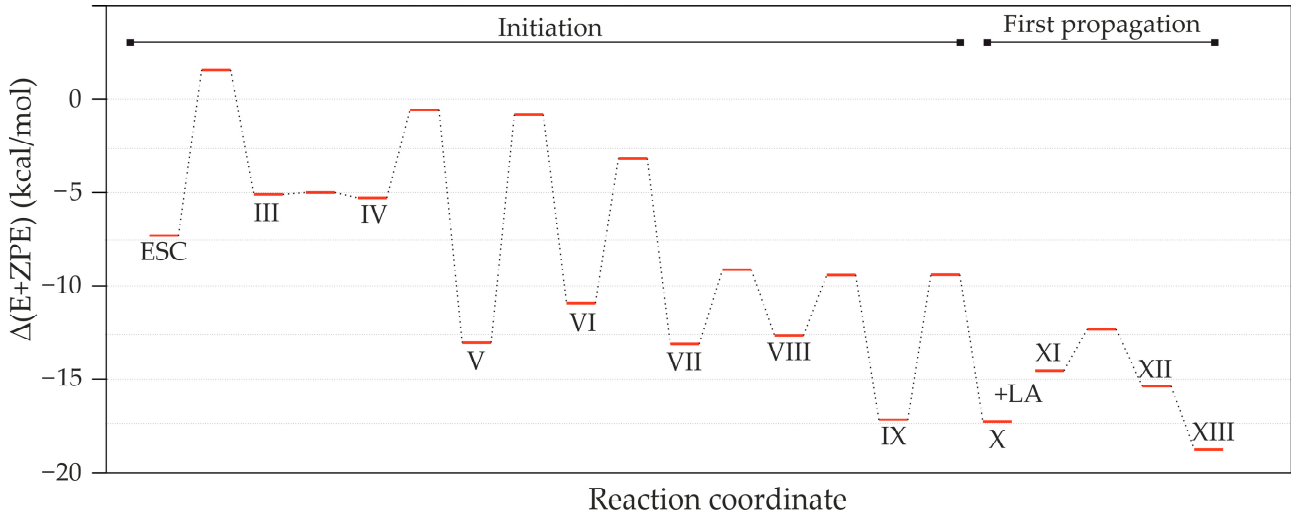

Figure 12. Energy profile of the initiation steps and the first cycle of PLA chain growth in the lactide ROP reaction catalyzed by a mononuclear mixed-ligand nickel(II) carboxylate. The sum of calculated energies of the separated **2** + DMA is set to 0.0 kcal/mol.

In order to check the possibility of the described reactions proceeding in the presence of real bulky substituents, calculations of the part of the previously modeled path **ESC→III→X** of the stage of initiation and opening of the lactide ring without the previously introduced simplifications (full model) using the relatively low-cost DFT method b97-3c were carried out. The energy profile of initiation of the lactide ring opening reaction obtained as a result of DFT modeling for the complete model system (Figure 13) is practically the same as that obtained for the simplified model. An attention-grabbing difference between the complete model system and the simplified one was a significant drop in the energy of the system after coordination of the lactide with the octahedral complex [Ni(DBED)($O_2CC(CH_3)_3$)$_2$] **I(f)** (the designation "f" means "full model"), which is 21.52 kcal/mol.

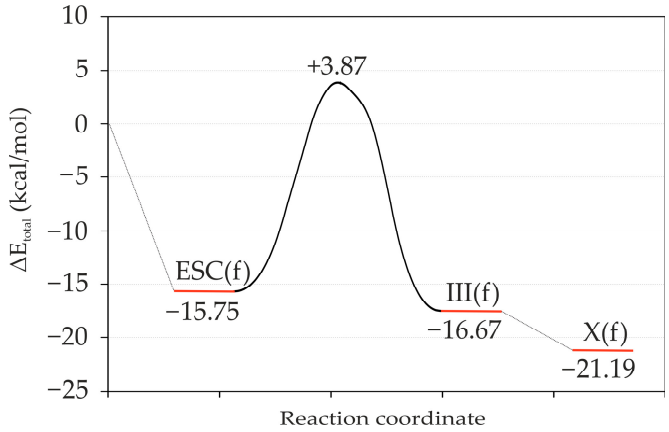

Figure 13. Energy profile for the initiation of the lactide ring opening reaction for the full model system. The sum of the calculated energies of the separated DBED + [Ni(DBED)(LA)($O_2CC(CH_3)_3$)$_2$] **II(f)** is set to 0.0 kcal/mol. The designation "f" means a structure of the corresponding number similar to the simplified model.

This difference can be explained by significant steric differences in the alkyl substituents in the models. It leads to a significant decrease in the energy of the system during lactide coordination and a change in the type of coordination of the pivalate ligand from bidentate-chelate to monodentate, which increases its mobility in the inner sphere of the model compound **II(f)**. When considering the **ESC(f)→III(f)** transition, we failed to obtain

an optimized TS structure. The energy barrier of this step was estimated by building the minimum energy path using the climbing image nudged elastic band method. The calculated value of the energy barrier was 19.61 kcal/mol, which is much larger than the value of the corresponding value for a similar energy barrier in the simplified model. In addition to steric hindrances in the **ESC(f)→III(f)** transition, the larger energy barrier can be explained by the formation of an extensive system of inter- and intramolecular non-covalent interactions between almost all ligands in the coordination environment of nickel and the DBED initiator, which "enchain" them and makes it difficult to rearrange the molecule.

In summary, the quantum chemical modeling of the lactide polymerization reaction pathway suggests that the proposed variant of initiating the polymerization reaction by DBED molecules that have left the inner coordination sphere of the metal ion is thermodynamically allowed. In a simplified model reaction, the energy barriers corresponding to the conformational changes of the monomer with the already broken ring exceed those for the stages of direct nucleophilic attack and C1-O2 bond cleavage within the lactide ring. It can be assumed that the presence of a bulky end group of the initiator and trimethyl acetate ligands, in reality, makes such conformational rearrangements even more difficult, which causes a relatively low catalytic activity of the compounds under study, despite the relatively low calculated values of energy barriers on the minimum energy path. In turn, the differences in the catalytic activity of compounds **1** and **2** can be explained in terms of the difference in the acidity of carboxylic acids, the anions of which are the carboxylate ligands used. During **III→VI** transitions, one of the key processes is the successive transfer of the H1 proton from the initiator molecule to the carboxylate ligand, the alkoxide end group being formed, and then back to the carboxylate. In the case of the trifluoroacetate ligand, compared to the pivalate ligand, this process should be more difficult.

2.4. Biological Evaluation

The successful application of biomaterials based on polyesters, including PLA, is possible if the catalyst used for their synthesis does not exhibit toxicity. In this regard, the in vitro cytotoxicity of complex **2** with higher catalytic properties in ROP of *rac*-LA was evaluated using mesenchymal stem cells (MSC) from the bone marrow (FetMSC cell line). The MTT assay was carried out for solutions of **2** taken at various concentrations in the range of 4–500 μg/mL for 24 h (Figure 14).

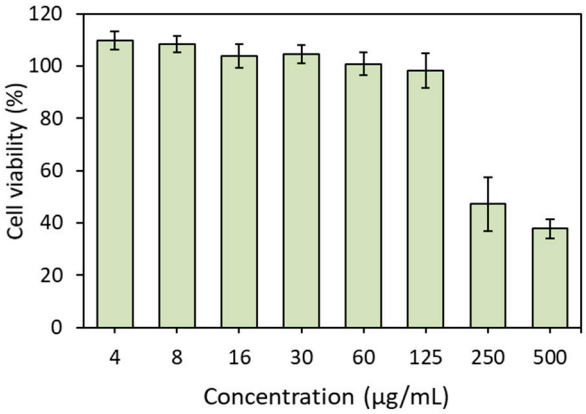

Figure 14. Cytotoxicity evaluation (MTT test, 24 h) in MSC for the complex **2** solution. Data presented as mean value ± SD (n = 3).

The examined complex revealed low cytotoxicity toward tested cells. Half-minimum inhibition concentration (IC_{50}) for the examined nickel(II) complex was 190 μg/mL.

3. Materials and Methods

3.1. Chemicals and Supplements

All starting materials and solvents for the synthesis of the complexes with a purity of more than 98% were purchased from Sigma-Aldrich (Darmstadt, Germany) and Vecton (St. Petersburg, Russia), respectively. Metal complex precursors $Ni(O_2CCF_3)_2{\cdot}4H_2O$ and $Ni_2((CH_3)_3CCO_2)_4((CH_3)_3CCO_2H)_4{\cdot}H_2O$ were synthesized according to the previously published procedures [92,93] from pre-prepared synthetic Hellyerite $NiCO_3{\cdot}5.5H_2O$ as described in [59].

Toluene (99%, Vecton, St. Petersburg, Russia) used for monomer purification and polymer synthesis was stored over 4 Å molecular sieves and then distilled over sodium metal immediately prior to use. *D,L*-lactide (*rac*-LA, 99%, Sigma-Aldrich, Darmstadt, Germany) was recrystallized twice from dry toluene and dried under vacuum to constant weight. Benzyl alcohol (BnOH, analytical grade, Vecton, St. Petersburg, Russia) used as the initiator was dried over freshly calcined CaO and distilled under reduced pressure.

Deuterated chloroform ($CDCl_3$) was a product of Solvex LLC (Moscow, Russia). Polystyrene (PS) calibration standards and HPLC grade tetrahydrofuran (THF) used as an eluent for size-exclusion chromatography (SEC) analysis were purchased from Waters (Milford, MA, USA) and Merck (Darmstadt, Germany), respectively.

The human bone marrow mesenchymal stem cell line (FetMSC) was received from the Vertebrate Cell Culture Collection of the Institute of Cytology RAS (St. Petersburg, Russia). Cells were cultured in humidified 5% CO_2 at 37 °C with the use of DMEM/F12 (Dulbecco's modified Eagle medium; Gibco, Grand Island, NY, USA) containing 1% non-essential amino acids (NEAA; Gibco, Grand Island, NY, USA), 10 vol% thermally inactivated fetal bovine serum (FBS; Hy-Clone, Logan, UT, USA), 1% L-glutamine (PanEco, Moscow, Russia), 50 U/mL penicillin (Sigma-Aldrich, Darmstadt, Germany), and 50 μg/mL streptomycin (Sigma-Aldrich, Darmstadt, Germany). MTT reagent (3-(4,5-dimethythiazol-2-yl)-2,5-diphenyl tetrazolium bromide) was a product of Sigma-Aldrich (St. Louis, MO, USA). In the study, 4–6 passage cells were used. Detachment of cells with trypsin-EDTA (Sigma-Aldrich, Darmstadt, Germany) was carried out at attaining 80% confluence.

3.2. Characterization Techniques

Elemental analysis of complexes was performed on a LECO CHNS(O)-932 elemental analyzer (LECO, Saint Joseph, MI, USA). Fourier transform infrared (FTIR) spectra were recorded using a Shimadzu IRTracer-100 spectrometer (Shimadzu, Kyoto, Japan) equipped with a Specac Quest attenuated total reflection (ATR) accessory (diamond crystal puck, Specac, Orpington, Kent, UK) in the range of 600 to 4000 cm^{-1} with a resolution of 1 cm^{-1}. Thermogravimetric analysis (TGA) was carried out using a Shimadzu DTG-60 (Shimadzu, Kyoto, Japan) and NETZSCH STA 449 F3 Jupiter (NETZSCH, Selb, Germany) instruments. The analyzed samples of the complexes (about 5 mg) were heated from 34 to 800 °C and from room temperature to 475 °C at a rate of 4 °C·min^{-1} in a flow of argon (99.995%, 100 mL·min^{-1}).

The Hirschfeld surface analysis [94] of the complexes was performed using the Crystal Explored 17.5 software [95].

Single crystal X-ray diffraction analyses of complexes **1**, **2** and **4** were carried out on an Xcalibur EOS diffractometer (Rigaku Oxford Diffraction, Oxford, UK) operated with monochromated Mo-K_α radiation (λ = 0.71073 Å) at a temperature of 100 K. Data were integrated and corrected for background, Lorentz, and polarization effects. An empirical absorption correction based on spherical harmonics implemented in the SCALE3 ABSPACK algorithm was applied in the *CrysAlisPro* program [96]. The structures were solved by a dual-space algorithm and refined using the *SHELX* programs [97,98] incorporated in the *OLEX2* program package [99]. The final models included coordinates and anisotropic displacement parameters for all non-H atoms. The carbon- and nitrogen-bound

H atoms were placed in calculated positions and were included in the refinement in the 'riding' model approximation, U_{iso}(H) set to 1.5U_{eq}(C) and C–H 0.98 Å for the CH_3 groups, U_{iso}(H) set to 1.2U_{eq}(C) and C–H 0.99 Å for the CH_2 groups, U_{iso}(H) set to 1.2U_{eq}(C) and C–H 0.95 Å for the CH groups of cyclic fragments, and U_{iso}(H) set to 1.2U_{eq}(N) and N–H 1.00 Å for the tertiary NH groups. The unit cell of compound **2** contains disordered pivalic acid molecules which have been treated as a diffuse contribution to the overall scattering without specific atom positions by SQUEEZE/PLATON [100]. The total approximate amount of four solvent molecules per unit cell in the structural model has been calculated taking into account the Electron Count of 233 and a Total Potential Solvent Accessible Void Volume of 870 e/A^3. Supplementary crystallographic data for this paper have been deposited at Cambridge Crystallographic Data Centre (CCDC 1546454, 1546456, 1840764 for **1**, **2** and **4**, respectively) and can be obtained free of charge via www.ccdc.cam.ac.uk/structures/ (accessed on 30 December 2022).

All mass spectrometry data were collected on a quadrupole time-of-flight LCMS-9030 system (Shimadzu, Kyoto, Japan) with electrospray ionization (ESI) technique in the ranges of 100–1000 *m*/*z* for complexes and oligomers of *rac*-LA. The instrument and method parameters were as follows: capillary voltage ±4 kV, drying gas (N_2) flow rate 10.0 L/min, heat block temperature 180 °C, acetonitrile (HPLC grade, JT Baker, Phillipsburg, NJ, USA).

Monomer conversions, number average and weight average molecular weights (M_n and M_w), and dispersity ($Đ$) of the polymers were determined by SEC using a HPLC Shimadzu System (Tokyo, Japan) consisting of a RID-10A refractometric detector, an FCV-10AL degasser, a LC-10AD VP pump, a CTO-20A column thermostat, a SCL-10A VP system controller and equipped with a Rheodyne 725i injection valve (Rohnert Park, CA, USA) and two Agilent PLgel MIXED-D columns (7.5 × 300 mm, 5 µm, Agilent Technologies, Santa Clara, CA, USA). The analysis was carried out at 40 °C using THF as the eluent at a flow rate of 1 mL/min. Column calibration was performed using PS standards (530–400,000). LC Solution Shimadzu 1.25 software (Kyoto, Japan) was used for SEC data analysis and to calculate polymer characteristics.

NMR spectra of the polymers before and after reprecipitation were recorded on an AVANCE AV-400 spectrometer (Bruker, Karlsruhe, Germany) at 298 K using TopSpin 2.1 software (Bruker BioSpin, Rheinstetten, Germany) for data processing. $CDCl_3$ was used as a deuterated solvent. The experimental chemical shifts (δ) for ^{1}H, ^{13}C NMR and one-dimensional diffusion ordered spectroscopy (1D DOSY) ^{1}H NMR were obtained in $CDCl_3$ and referenced using residual proton or carbon signals of the deuterated solvent and reported in ppm.

3.3. Synthesis of Nickel(II) Complexes

3.3.1. Preparation of *trans*-[Ni(DBED)$_2$(O_2CCF_3)$_2$]·C_6H_6 (1)

N,*N*′-dibenzylethylenediamine (DBED, 0.233 mL, 1.000 mmol) and benzene (35 mL) were added to a pre-prepared solution of Ni(O_2CCF_3)$_2$·4H_2O (0.3568 g, 1.000 mmol) in methanol (40 mL) at room temperature. Then, the reaction mixture was refluxed for 1 h. The resulting solution was cooled and slowly concentrated at room temperature, affording blue rhombic crystals after about 3 days.

Yield 85% (0.351 g, 0.41 mmol). Anal. Calcd for $C_{42}H_{46}F_6N_4O_4Ni$ (843.54 g/mol): C 59.80; H 5.50; N 6.64%; found: C 59.9; H 5.2; N 6.7%. FTIR (ATR, cm^{-1}): 3331 (s), 3279 (s), 2970 (vs), 2932 (s), 2872 (m), 1731 (s), 1706 (s), 1545 (vs), 1481 (vs), 1454 (s), 1414 (vs), 1372 (m), 1360 (m), 1274 (s), 1226 (m), 1182 (vs), 1126 (w), 1002 (w), 986 (w), 901 (s), 747 (vs), 702 (vs). Structural data: *P*-1; a = 8.9998(2), b = 9.3083(2), c = 13.4098(3) Å; α = 95.568(2), β = 90.678(2), γ = 113.699(2)°; V = 1022.19(5) Å^3; Z = 1; R_1 = 3.4%; CCDC 1546454.

3.3.2. Preparation of *trans*-[Ni(DBED)$_2$(O$_2$CC(CH$_3$)$_3$)$_2$]·(CH$_3$)$_3$CCO$_2$H (2)

The synthesis of complex **2** was carried out according to a similar procedure as for complex **1**, but with some changes. Two equivalents of DBED (0.990 mL, 4.227 mmol) and 40 mL of hexane were added to a solution of Ni$_2$((CH$_3$)$_3$CCO$_2$)$_4$((CH$_3$)$_3$CCO$_2$H)$_4$·H$_2$O (2.000 g, 2.113 mmol) in 40 mL of THF and the mixture was heated at 60 °C for 1 h. Subsequent prolonged (about 5 days) concentration of the blue solution obtained by gentle evaporation in air at room temperature to reduce the volume of the mixture by about 4–5 times and standing in a refrigerator (+4 °C) for 1 day resulted in blue prismatic crystals of complex **2**.

Yield 30% (1.13 g, 1.14 mmol). Anal. Calcd for C$_{47}$H$_{68}$N$_4$NiO$_6$ (741.63 g/mol): C 66.90; H 8.12; N 6.64%; found C 67.1; H 7.9; N 6.8%. FTIR (ATR, cm^{-1}): 3325 (w), 3187 (m), 2941 (m), 2883 (w), 1681 (vs), 1493 (w), 1455 (m), 1431 (m), 1379 (w), 1340 (w), 1291 (w), 1200 (vs), 1131 (vs), 1087 (w), 1063 (s), 1020 (m), 934 (m), 917 (m), 840 (m), 805 (m), 753 (s), 725 (m), 698 (s), 618 (m). Structural data: $P2_1/n$; a = 14.1992(6), b = 11.4582(3), c = 17.4222(7) Å; β = 106.633(4)°; V = 2715.94(18) Å^3; Z = 2; R_1 = 6.0%; CCDC 1546456.

3.3.3. Preparation of [Ni$_2$(μ-OH$_2$)(μ-O$_2$CCF$_3$)$_2$(O$_2$CCF$_3$)$_2$(TEMED)$_2$] (3) and [Ni$_2$(μ-OH$_2$)(μ-O$_2$CC$_6$H$_5$)$_2$(O$_2$CC$_6$H$_5$)$_2$(TEMED)$_2$] (4)

Binuclear complexes **3** and **4** containing TEMED (*N*,*N*,*N*′,*N*′-tetramethylethylenediamine) ligand were synthesized according to [61] and [60], respectively, without changes. However, **4** was obtained for the first time and was not previously described in the literature. Briefly, benzoic acid was added to a suspension of NiCO$_3$·5.5H$_2$O (0.6534 g, 3 mmol) in 100 mL of acetonitrile-water (20/1 *v*/*v*) and the mixture was stirred at 50 °C for 1 h. Then, TEMED was added to the reaction system. Subsequent slow evaporation in the air (about 7 days) of the resulting bright green solution led to the formation of green rhombic crystals of complex **4**.

The yield of [Ni$_2$(μ-OH$_2$)(μ-O$_2$CC$_6$H$_5$)$_2$(O$_2$CC$_6$H$_5$)$_2$(TEMED)$_2$] 35% (1.79 g, 2.1 mmol). Anal. Calcd for C$_{40}$H$_{54}$N$_4$Ni$_2$O$_9$ (852.29 g/mol): C 56.37; H 6.39; N 6.57%; found: C 56.2; H 6.5; N 6.4%. FTIR (ATR, cm^{-1}): 3061 (w), 3019 (w), 2984 (w), 2885 (m), 2841 (m), 1632 (s), 1577 (m), 1527 (m), 1460 (m), 1392 (vs), 1287 (w), 1169 (m), 1126 (m), 1066 (m), 1024 (s), 1014 (m), 955 (m), 825 (s), 803 (s), 712 (vs), 673 (vs), 588 (m). Structural data: *P*-1; a = 10.7368(6), b = 11.6727(7), c = 17.0611(8) Å; α = 106.054(5), β = 91.296(4), γ = 93.786(5)°; V = 2048.48(19) Å^3; Z = 2; R_1 = 4.1%; CCDC 1840764.

3.4. Protocol of rac-LA Polymerization

The polymerization reaction of *rac*-lactide was carried out via ROP of the monomer using two different strategies, namely with and without the addition of benzyl alcohol as an initiator to the system containing nickel catalyst and monomer. In addition, both bulk and solution polymerization of the monomer were studied. All polymerization reactions were carried out under an inert atmosphere in sealed ampoules using standard Schlenk techniques. The ampoules were dried at 180 °C and cooled in a vacuum immediately before use.

In the case of solution polymerization, pre-purified *rac*-LA (500 mg), an appropriate amount of solid Ni^{II} complex, BnOH (if required) and 2 mL of freshly dried toluene were placed into glass ampoules (15 mL). The resulting mixtures were degassed using the freeze-pump-thaw cycling technique, filled with argon, and sealed. In the case of bulk polymerization, the polymerization mixture was prepared in a 10 mL ampoule in exactly the same way as in the previous case, but without the addition of BnOH and toluene. The ampoule was also filled with argon and then sealed. All ampoules after sealing were incubated at selected conditions. All polymerization mixtures at the studied temperatures were homogeneous. The investigated monomer/catalyst/initiator ratios, polymerization temperatures and times are presented in Tables 1 and 2 and Figure 4.

After the specified polymerization time, the ampoules were opened and the systems obtained by bulk polymerization were dissolved by adding 3 mL of THF, while the reaction solutions in toluene were left unchanged. Aliquots were taken from the obtained solutions of both types, diluted with THF to obtain polylactide concentrations of ~6 mg/mL, and studied by SEC analysis to evaluate the monomer conversions and molecular weight characteristics of the polymers. The remaining parts of the resulting toluene solutions of the polymers were precipitated in a ~50-fold excess of ice-cold ethanol, separated by centrifugation, washed twice with ethanol, and dried under vacuum at 40 °C to constant weight. After that, they were analyzed in the form of solutions in $CDCl_3$ by ^1H and 1D DOSY ^1H NMR to determine the terminal groups of the polymers.

Model systems of *rac*-LA oligomers were prepared under conditions similar to the polymerization of *rac*-lactide in toluene solution (200 mg *rac*-LA, 2 mL solvent, synthesis 72 h at 140 °C), but using low [*rac*-LA]/[Ni] ratios (2/1 or 3/1, respectively) and without the addition of BnOH. After polymerization without any manipulations, these systems were used to study the mechanism of polymerization by ESI mass spectrometry.

3.5. Density Functional Theory (DFT) Calculation Details

All DFT calculations were performed using the ORCA program system (ver. 5.0.1 and 4.2.1, https://orcaforum.kofo.mpg.de/, accessed on 21 February 2022) [101,102]. Energies and geometries were evaluated by means of DFT PBE0 [103] and B97-3c [104] methods using def2-SVP basis set [105] in the gas phase at 298.15 K and 1 atm. The application of the DFT PBE0 method shows good results, consistent with experimental data, in calculations of the structural and magnetic characteristics of Ni(II) coordination compounds with carboxylate and N-donor ligands [69,106]. In the present work, we used the PBE0 method for a detailed description of the reaction mechanism and the relatively low-cost B97-3c DFT method to calculate the full model. Transition states were localized either based on the initial potential energy surface (PES) scan (relaxed surface scan method) or using the nudged elastic band method [107–109]. L-lactide was used as a monomer for computational reasons.

3.6. Biological Evaluation

The cytotoxicity exhibited by complex **2** was assessed by the cell viability of mesenchymal stem (FetMSC) cells using the MTT assay. Before the experiment, the solid-state complex was sterilized under wide-spectrum UV-light for 15 min. The study was carried out for solutions with concentrations in the range of 4–500 μg/mL. Since the solubility of the complex under study is limited in aqueous media, 5% DMSO by volume was added to the starting solution (500 μg/mL), from which a series of double-diluted solutions were prepared. A control complex-free system contained a similar amount of DMSO dissolved in the cell culture medium (n = 3).

Preliminary, 5×10^3 cells (100 μL) per well were seeded in an adhesive 96-well plate and cultured for 24 h for their attachment. Then, the medium was removed and 100 μL/well of complete DMEM/F12 culture medium containing complex **2** at the test concentration was added (n = 3). After 24 h of incubation, MTT reagent solution (0.1 mg/mL, 50 μL/well) was added to each well and the plate was incubated with 5% CO_2 at 37 °C for 2 h. After removal of the supernatant, formed formazan crystals were dissolved in DMSO (50 μL/well). The absorbance of the obtained purple solutions was measured at 570 nm in a Thermo Fisher Multiscan Labsystems plate reader (Waltham, MA, USA). The calculations and visualization of the obtained results were performed using the MS Excel software (Microsoft, Redmond, Washington, DC, USA).

4. Conclusions

A number of new mononuclear and binuclear nickel(II) complexes were synthesized and characterized by X-ray diffraction analysis. The obtained nickel(II) complexes

containing various ethylenediamine derivatives (*N*,*N*′-dibenzylethylenediamine—DBED and *N*,*N*,*N*′,*N*′-tetramethylethylenediamine) and carboxylate ligands ($O_2CC(CH_3)_3$, O_2CCF_3, $O_2CC_6H_5$) are characterized by an octahedral metal core and differ in the rigidity, steric properties and nature of the carboxylate ligands. The ring-opening polymerization of *rac*-lactide catalyzed by nickel(II) carboxylate complexes in bulk and in solution was investigated. An increase in catalytic ability in *rac*-lactide ROP was observed for compounds with lower rigidity of the metal core and higher basicity of the carboxylate ligands. Due to the presence of labile N-donor ligands, the complexes studied can catalyze and initiate the polymerization reaction with a secondary amine leaving the inner sphere of the complex, which was confirmed by ESI mass spectrometry and ^{1}H and 1D DOSY ^{1}H NMR spectroscopy. For the $[Ni(DBED)_2(O_2CC(CH_3)_3)_2]\cdot((CH_3)_3CCO_2)_2$ complex, which exhibited the best catalytic properties, the ROP reaction pathway including the initiation and first chain growth cycle steps, was studied by a comprehensive DFT method. The intermediates and energy barriers of the reaction steps were estimated and described in detail. The performed quantum-chemical modeling of the ROP pathway of lactide confirmed the possibility of the proposed initiation process. In addition, it was revealed that one of the key roles is played by carboxylate ligands, which act as proton carriers from the initiator molecule and have a significant influence on the catalytic ability of metal complexes. In vitro biological evaluation of the $[Ni(DBED)_2(O_2CC(CH_3)_3)_2]\cdot(CH_3)_3CCO_2)_2$ complex demonstrated low cytotoxicity in mesenchymal stem cells.

Supplementary Materials: The following supporting information can be downloaded at: www.mdpi.com/xxx/s1. Figure S1: C-H···F and N-H···F close contacts in crystal structure of **1**; Figure S2: Network system C-H···O hydrogen bonds of complex units with solvate molecules of benzene in the crystal structure of compound **1**; Figure S3: Hirshfeld surfaces (HS) of complex **1** over the d_{norm} map in the range −0.2399–1.5851 a.u.; Figure S4: Fragment of the crystal structure of $[Ni_2(\mu\text{-}OH_2)(\mu\text{-}O_2CC_6H_5)_2(O_2CC_6H_5)_2(TEMED)_2]$ (TEMED—*N*,*N*,*N*′,*N*′-tetramethylethylenediamine)—**4**: offset-face-to-face π···π stacking interactions of phenyl substituents of benzoate ligands; Figure S5: Fragment of the crystal structure of complex **4**: C-H···π face-to-plane interactions of phenyl substituents of benzoate ligands (the compound unit cell is shown); Figure S6: HS of **4**: (a) over the d_{norm} map in the range −0.1278–1.5984 a.u, (b) over the shape index map; Figure S7: Thermogravimetric analysis (TGA) of complex **1**; Figure S8: TGA of complex **2**; Figure S9: Simultaneous thermal analysis of complex **4**; Figure S10: Fragment of carbonyl region of ^{13}C NMR spectrum in $CDCl_3$ of precipitated poly-*D*,*L*-lactide, obtained with compound **2**. Reaction conditions: [*rac*-lactide]/[Ni] 250/1, toluene, 72 h, 140 °C, argon atmosphere; Figure S11: Proposed transformation pathway of DBED ligand (a) and structure of $[(DBED)(Lac)_n(CO)]$ formylated dialkyl lactamide species (b) in ESI mass spectrometry experiment; Figures S12: ESI mass-spectra of **1** (a) and **2** (b); Figures S13: Electrospray ionization mass-spectra of model polymerization mixtures ([*rac*-lactide]/[Ni]—3/1, toluene, 72 h, 140 °C, argon atmosphere): (a) general view (100–1000 *m*/*z*), (b) part of the spectrum (338–538 *m*/*z*), (**c**) part of the spectrum (532–635 *m*/*z*), (d) part of the spectrum (628–731 *m*/*z*), (e) part of the spectrum (728–831 *m*/*z*), (f) (824–1000 *m*/*z*); Figure S14: ^{1}H 1D DOSY NMR spectrum in $CDCl_3$ of precipitated poly-D,L-lactide, obtained with compound **2** (gradient intensity 90%). Reaction conditions: [*rac*-lactide]/[Ni] 250/1, toluene, 72 h, 140 °C, argon atmosphere; Figure S15: Optimized structure of the **X** compound. Bond lengths are given in Å; Figure S16: Optimized structure of the **XI** compound. Bond lengths are given in Å; Figure S17: Optimized structure of the **XIII** compound. Bond lengths are given in Å; Table S1: Geometric parameters of intramolecular hydrogen bonds in compounds *trans*-$[Ni(DBED)_2(O_2CCF_3)_2]\cdot C_6H_6$—**1** and *trans*-$[Ni(DBED)_2(O_2CC(CH_3)_3)_2]\cdot(CH_3)_3CCO_2H$—**2** (DBED—*N*,*N*′-dibenzylethylenediamine); Table S2: Some values of average Ni-N and Ni-O bond lengths for complexes **1**–**4**; Table S3: Calculated molecular formulas and masses of dialkyl lactamide species in electrospray ionization (ESI) mass-spectra of model reaction mixture ([*rac*-lactide]/[Ni]—3/1, toluene, 72 h, 140 °C, argon atmosphere).

Author Contributions: Conceptualization, A.E. and M.S.; methodology, A.N., N.P., V.G., A.E. and M.S.; investigation, A.N., N.P., D.B., V.G. and J.N.; resources, V.G., N.P., A.E. and E.K.-V.; formal analysis, A.N., N.P., A.E. and M.S.; data curation, M.S. and A.N.; writing—original draft preparation, A.N., N.P., A.E. and M.S.; writing—review and editing, A.N., E.K.-V., A.E., N.P. and M.S.; visualization, A.N. and A.E.; supervision, M.S.; project administration, E.K.-V. All authors have read and agreed to the published version of the manuscript.

Funding: The research of authors from IMC RAS was funded by the Ministry of Science and Higher Education of the Russian Federation as a part of the State Assignment of IMC RAS, project no. AAAA-A20-120022090039-8. The author from SPbU (E.K.-V.) thanks the Ministry of Science and Higher Education of the Russian Federation for financial support in the frames of Megagrant, project no. 075-15-2021-637.

Data Availability Statement: The supplementary crystallographic data of the obtained complexes can be found free of charge on the Cambridge Crystallographic Data Center via https://www.ccdc.cam.ac.uk/structures/ (accessed on 30 December 2022). Deposition numbers 1546454 (**1**), 1546456 (**2**), 1840764 (**4**). Other data are available within the article and its Supplementary Materials.

Acknowledgments: N.P. thanks SPbSTI(TU) for FT-IR and thermal analysis (Engineering Center) and for access to computer resources (High-Performance Computing Center). The authors express their deep gratitude to A.I. Panin and A.V. Dobrodumov for their significant help in obtaining and interpreting the DFT calculation data and NMR spectra, respectively. V.G. and E.K.-V. thank the Research Park of SPbU for XRD (X-ray Diffraction Center) and mass-spectrometry studies (Chemical Analysis and Materials Research Center).

Conflicts of Interest: The authors declare no conflict of interest.

References

1. Prokop, A.; Jubel, A.; Helling, H.J.; Eibach, T.; Peters, C.; Baldus, S.E.; Rehm, K.E. Soft Tissue Reactions of Different Biodegradable Polylactide Implants. *Biomaterials* **2004**, *25*, 259–267. https://doi.org/10.1016/S0142-9612(03)00496-4.
2. Moetazedian, A.; Gleadall, A.; Han, X.; Silberschmidt, V.V. Effect of Environment on Mechanical Properties of 3D Printed Polylactide for Biomedical Applications. *J. Mech. Behav. Biomed. Mater.* **2020**, *102*, 103510. https://doi.org/10.1016/j.jmbbm.2019.103510.
3. Averianov, I.; Stepanova, M.; Gofman, I.; Lavrentieva, A.; Korzhikov-Vlakh, V.; Korzhikova-Vlakh, E. Osteoconductive Biocompatible 3D-Printed Composites of Poly-D,L-Lactide Filled with Nanocrystalline Cellulose Modified by Poly(Glutamic Acid). *Mendeleev Commun.* **2022**, *32*, 810–812. https://doi.org/10.1016/j.mencom.2022.11.034.
4. Stepanova, M.; Averianov, I.; Solomakha, O.; Zabolotnykh, N.; Gofman, I.; Serdobintsev, M.; Vinogradova, T.; Korzhikov-Vlakh, V.; Korzhikova-Vlakh, E. Composite Biomaterials Based on Poly(L-Lactic Acid) and Functionalized Cellulose Nanocrystals. *J. Renew. Mater.* **2020**, *8*, 383–395. https://doi.org/10.32604/jrm.2020.09206.
5. Xiao, X.; Chevali, V.S.; Song, P.; He, D.; Wang, H. Polylactide/Hemp Hurd Biocomposites as Sustainable 3D Printing Feedstock. *Compos. Sci. Technol.* **2019**, *184*, 107887. https://doi.org/10.1016/j.compscitech.2019.107887.
6. Averianov, I.; Stepanova, M.; Solomakha, O.; Gofman, I.; Serdobintsev, M.; Blum, N.; Kaftuirev, A.; Baulin, I.; Nashchekina, J.; Lavrentieva, A.; et al. 3D-Printed Composite Scaffolds Based on Poly(ε-caprolactone) Filled with Poly(Glutamic Acid)-modified Cellulose Nanocrystals for Improved Bone Tissue Regeneration. *J. Biomed. Mater. Res. B Appl. Biomater.* **2022**, *110*, 2422–2437. https://doi.org/10.1002/jbm.b.35100.
7. Calzoni, E.; Cesaretti, A.; Polchi, A.; di Michele, A.; Tancini, B.; Emiliani, C. Biocompatible Polymer Nanoparticles for Drug Delivery Applications in Cancer and Neurodegenerative Disorder Therapies. *J. Funct. Biomater.* **2019**, *10*, 4. https://doi.org/10.3390/jfb10010004.
8. Chen, W.; Zhou, S.; Ge, L.; Wu, W.; Jiang, X. Translatable High Drug Loading Drug Delivery Systems Based on Biocompatible Polymer Nanocarriers. *Biomacromolecules* **2018**, *19*, 1732–1745. https://doi.org/10.1021/acs.biomac.8b00218.
9. Stepanova, M.; Dobrodumov, A.; Averianov, I.; Gofman, I.; Nashchekina, J.; Guryanov, I.; Klyukin, I.; Zhdanov, A.; Korzhikova-Vlakh, E.; Zhizhin, K. *Polymers* **2022**, *14*, 3864. https://doi.org/10.3390/polym14183864.
10. Ahmed, J.; Mulla, M.Z.; Al-Zuwayed, S.A.; Joseph, A.; Auras, R. Morphological, Barrier, Thermal, and Rheological Properties of High-Pressure Treated Co-Extruded Polylactide Films and the Suitability for Food Packaging. *Food Packag. Shelf Life* **2022**, *32*, 100812. https://doi.org/10.1016/j.fpsl.2022.100812.
11. Naser, A.Z.; Deiab, I.; Darras, B.M. Poly(Lactic Acid) (PLA) and Polyhydroxyalkanoates (PHAs), Green Alternatives to Petroleum-Based Plastics: A Review. *RSC Adv.* **2021**, *11*, 17151–17196. https://doi.org/10.1039/D1RA02390J.
12. Freeland, B.; McCarthy, E.; Balakrishnan, R.; Fahy, S.; Boland, A.; Rochfort, K.D.; Dabros, M.; Marti, R.; Kelleher, S.M.; Gaughran, J. A Review of Polylactic Acid as a Replacement Material for Single-Use Laboratory Components. *Materials* **2022**, *15*, 2989. https://doi.org/10.3390/ma15092989.
13. Stepanova, M.; Korzhikova-Vlakh, E. Modification of Cellulose Micro- and Nanomaterials to Improve Properties of Aliphatic Polyesters/Cellulose Composites: A Review. *Polymers* **2022**, *14*, 1477. https://doi.org/10.3390/polym14071477.
14. Auras, R.; Lim, L.T.; Selke, S.E.M.; Tsuji, H. *Poly(Lactic Acid): Synthesis, Structures, Properties, Processing, and Applications*; John Wiley & Sons, Inc.: Hoboken, NJ, USA, 2010; p. 432. https://doi.org/10.1002/9780470649848.
15. Moins, S.; Hoyas, S.; Lemaur, V.; Orhan, B.; Chiaie, K.D.; Lazzaroni, R.; Taton, D.; Dove, A.P.; Coulembier, O. Stereoselective Rop of Rac-and Meso-Lactides Using Achiral Tbd as Catalyst. *Catalysts* **2020**, *10*, 620. https://doi.org/10.3390/catal10060620.

16. Leenslag, J.W.; Pennings, A.J. Synthesis of High-Molecular-Weight Poly(L-Lactide) Initiated with Tin 2-Ethylhexanoate. *Die Makromol. Chem.* **1987**, *188*, 1809–1814. https://doi.org/10.1002/macp.1987.021880804.
17. Schwach, G.; Coudane, J.; Engel, R.; Vert, M. More about the Polymerization of Lactides in the Presence of Stannous Octoate. *J. Polym. Sci. A Polym. Chem.* **1997**, *35*, 3431–3440. https://doi.org/10.1002/(SICI)1099-0518(19971130)35:16<3431::AID-POLA10>3.0.CO;2-G.
18. Dubois, P.; Jacobs, C.; Jérôme, R.; Teyssté, P. Macromolecular Engineering of Polylactones and Polylactides. 4. Mechanism and Kinetics of Lactide Homopolymerization by Aluminum Isopropoxide. *Macromolecules* **1991**, *24*, 2266–2270. https://doi.org/10.1021/ma00009a022.
19. Dechy-Cabaret, O.; Martin-Vaca, B.; Bourissou, D. Controlled Ring-Opening Polymerization of Lactide and Glycolide. *Chem. Rev.* **2004**, *104*, 6147–6176. https://doi.org/10.1021/cr040002s.
20. Fuoco, T.; Pappalardo, D. Aluminum Alkyl Complexes Bearing Salicylaldiminato Ligands: Versatile Initiators in the Ring-Opening Polymerization of Cyclic Esters. *Catalysts* **2017**, *7*, 64. https://doi.org/10.3390/catal7020064.
21. Dubey, S.; Abhyankar, H.; Marchante, V.; Brighton, J.; Blackburn, K. Chronological Review of the Catalytic Progress of Polylactic Acid Formation through Ring Opening Polymerization. *Int. Res. J. Pure Appl. Chem.* **2016**, *12*, 1–20. https://doi.org/10.9734/IRJPAC/2016/27469.
22. Mezzasalma, L.; Dove, A.P.; Coulembier, O. Organocatalytic Ring-Opening Polymerization of l-Lactide in Bulk: A Long Standing Challenge. *Eur. Polym. J.* **2017**, *95*, 628–634. https://doi.org/10.1016/j.eurpolymj.2017.05.013.
23. Lewinski, P.; Sosnowski, S.; Penczek, S. L-Lactide Polymerization—Living and Controlled—Catalyzed by Initiators: Hydroxyalkylated Organic Bases. *Polymer* **2017**, *108*, 265–271. https://doi.org/10.1016/j.polymer.2016.11.070.
24. Lewinski, P.; Kaluzynski, K.; Pretula, J.; Mielniczak, G.; Penczek, S. Catalysis in Polymerization of Cyclic Esters. Catalyst and Initiator in One Molecule. Polymerization of Lactide. *J. Catal.* **2022**, *405*, 249–264. https://doi.org/10.1016/j.jcat.2021.11.038.
25. Gadomska-Gajadhur, A.; Ruśkowski, P. Biocompatible Catalysts for Lactide Polymerization—Catalyst Activity, Racemization Effect, and Optimization of the Polymerization Based on Design of Experiments. *Org. Process Res. Dev.* **2020**, *24*, 1435–1442. https://doi.org/10.1021/acs.oprd.0c00149.
26. Zhang, L.; Pratt, R.C.; Nederberg, F.; Horn, H.W.; Rice, J.E.; Waymouth, R.M.; Wade, C.G.; Hedrick, J.L. Acyclic Guanidines as Organic Catalysts for Living Polymerization of Lactide. *Macromolecules* **2010**, *43*, 1660–1664. https://doi.org/10.1021/ma901776x.
27. Liu, N.; Gu, C.; Chen, M.; Zhang, J.; Yang, W.; Zhan, A.; Zhang, K.; Lin, Q.; Zhu, L. Terpolymerizations of CO_2, Propylene Oxide and DL-Lactide Catalyzed by Zn-Fe DMC Catalysts with Quaternary Ammonium Salts. *ChemistrySelect* **2020**, *5*, 2388–2394. https://doi.org/10.1002/slct.201904461.
28. Schäfer, P.M.; Herres-Pawlis, S. Robust Guanidine Metal Catalysts for the Ring-Opening Polymerization of Lactide under Industrially Relevant Conditions. *ChemPlusChem* **2020**, *85*, 1044–1052. https://doi.org/10.1002/cplu.202000252.
29. Kricheldorf, H.R.; Weidner, S.M. High Molecular Weight Poly(*L*-lactide) via ring-opening Polymerization with Bismuth Subsalicylate—The Role of Cocatalysts. *J. Appl. Polym. Sci.* **2021**, *138*, 50394. https://doi.org/10.1002/app.50394.
30. Myers, M.; Connor, E.F.; Glauser, T.; Möck, A.; Nyce, G.; Hedrick, J.L. Phosphines: Nucleophilic Organic Catalysts for the Controlled Ring-Opening Polymerization of Lactides. *J. Polym. Sci. A Polym. Chem.* **2002**, *40*, 844–851. https://doi.org/10.1002/pola.10168.
31. Luo, Z.; Chaemchuen, S.; Zhou, K.; Verpoort, F. Ring-Opening Polymerization of *L*-Lactide to Cyclic Poly(Lactide) by Zeolitic Imidazole Framework ZIF-8 Catalyst. *ChemSusChem* **2017**, *10*, 4135–4139. https://doi.org/10.1002/cssc.201701438.
32. Rentero, C.; Damián, J.; Medel, A.; Fernández-Millán, M.; Rusconi, Y.; Talarico, G.; Cuenca, T.; Sessini, V.; Mosquera, M.E.G. Ring-Opening Polymerization of *L*-Lactide Catalyzed by Potassium-Based Complexes: Mechanistic Studies. *Polymers* **2022**, *14*, 2982. https://doi.org/10.3390/polym14152982.
33. Kremer, A.B.; Mehrkhodavandi, P. Dinuclear Catalysts for the Ring Opening Polymerization of Lactide. *Coord. Chem. Rev.* **2019**, *380*, 35–57. https://doi.org/10.1016/j.ccr.2018.09.008.
34. Wu, L.-J.; Lee, W.; Kumar Ganta, P.; Chang, Y.-L.; Chang, Y.-C.; Chen, H.-Y. Multinuclear Metal Catalysts in Ring-Opening Polymerization of ε-caprolactone and Lactide: Cooperative and Electronic Effects between Metal Centers. *Coord. Chem. Rev.* **2023**, *475*, 214847. https://doi.org/10.1016/j.ccr.2022.214847.
35. Wang, H.; Cue, J.M.O.; Calubaquib, E.L.; Kularatne, R.N.; Taslimy, S.; Miller, J.T.; Stefan, M.C. Neodymium Catalysts for Polymerization of Dienes, Vinyl Monomers, and ε-Caprolactone. *Polym. Chem.* **2021**, *12*, 6790–6823. https://doi.org/10.1039/D1PY01270C.
36. Kricheldorf, H.R.; Serra, A. Polylactones. *Polym. Bull.* **1985**, *14*, 497–502. https://doi.org/10.1007/BF00271606.
37. Khononov, M.; Liu, H.; Fridman, N.; Tamm, M.; Eisen, M.S. Mono(Imidazolin-2-Iminato) Hafnium Complexes: Synthesis and Application in the Ring-Opening Polymerization of ε-Caprolactone and *rac*-Lactide. *Catalysts* **2022**, *12*, 1201. https://doi.org/10.3390/catal12101201.
38. Zhang, X.; Prior, T.J.; Chen, K.; Santoro, O.; Redshaw, C. Ring Opening Polymerization of Lactides and Lactones by Multimetallic Titanium Complexes Derived from the Acids $Ph_2C(X)CO_2H$ (X = OH, NH_2). *Catalysts* **2022**, *12*, 935. https://doi.org/10.3390/catal12090935.
39. Jenkins, D.T.; Fazekas, E.; Patterson, S.B.H.; Rosair, G.M.; Vilela, F.; McIntosh, R.D. Polymetallic Group 4 Complexes: Catalysts for the Ring Opening Polymerisation of Rac-Lactide. *Catalysts* **2021**, *11*, 551. https://doi.org/10.3390/catal11050551.

40. Rosen, T.; Rajpurohit, J.; Lipstman, S.; Venditto, V.; Kol, M. Isoselective Polymerization of *rac*-Lactide by Highly Active Sequential {ONNN} Magnesium Complexes. *Chem. Eur. J.* **2020**, *26*, 17183–17189. https://doi.org/10.1002/chem.202003616.
41. Devaine-Pressing, K.; Oldenburg, F.J.; Menzel, J.P.; Springer, M.; Dawe, L.N.; Kozak, C.M. Lithium, Sodium, Potassium and Calcium Amine-Bis(Phenolate) Complexes in the Ring-Opening Polymerization of *rac*-Lactide. *Dalton Trans.* **2020**, *49*, 1531–1544. https://doi.org/10.1039/c9dt04561a.
42. Chandanabodhi, D.; Nanok, T. A DFT Study of the Ring-Opening Polymerization Mechanism of *L*-Lactide and ϵ-Caprolactone Using Aluminium Salen-Type Initiators: Towards an Understanding of Their Reactivities in Homo- and Copolymerization. *Mol. Catal.* **2017**, *436*, 145–156. https://doi.org/10.1016/j.mcat.2017.04.005.
43. Nifant'ev, I.E.; Shlyakhtin, A.V.; Bagrov, V.V.; Minyaev, M.E.; Churakov, A.V.; Karchevsky, S.G.; Birin, K.P.; Ivchenko, P.V. Mono-BHT Heteroleptic Magnesium Complexes: Synthesis, Molecular Structure and Catalytic Behavior in the Ring-Opening Polymerization of Cyclic Esters. *Dalton Trans.* **2017**, *46*, 12132–12146. https://doi.org/10.1039/c7dt02469j.
44. Jitonnom, J.; Meelua, W. DFT Study of Lactide Ring-Opening Polymerizations by Aluminium Trialkoxides: Understanding the Effects of Monomer, Alkoxide Substituent, Solvent and Metal. *Chem. Phys. Lett.* **2020**, *750*, 137482. https://doi.org/10.1016/j.cplett.2020.137482.
45. Ozen, C.; Satoh, T.; Maeda, S. A Theoretical Study on the Alkali Metal Carboxylate-Promoted L-Lactide Polymerization. *J. Comput. Chem.* **2020**, *41*, 2197–2202. https://doi.org/10.1002/jcc.26386.
46. Albertsson, A.C.; Varma, I.K. Recent Developments in Ring Opening Polymerization of Lactones for Biomedical Applications. *Biomacromolecules* **2003**, *4*, 1466–1486. https://doi.org/10.1021/bm034247a.
47. Kricheldorf, H.R.; Kreiser-Saunders, I.; Stricker, A. Polylactones 48. $SnOct_2$-Initiated Polymerizations of Lactide: A Mechanistic Study. *Macromolecules* **2000**, *33*, 702–709. https://doi.org/10.1021/ma991181w.
48. Ogoshi, S. *Nickel Catalysis in Organic Synthesis: Methods and Reactions*; Wiley-VCH: Weinheim, Germany, 2019; p. 352. https://doi.org/10.1002/9783527813827.
49. Tasker, S.Z.; Standley, E.A.; Jamison, T.F. Recent Advances in Homogeneous Nickel Catalysis. *Nature* **2014**, *509*, 299–309. https://doi.org/10.1038/nature13274.
50. Zhang, X.; Qi, D.; Jiao, C.; Liu, X.; Zhang, G. Nickel-Catalyzed Deaminative Sonogashira Coupling of Alkylpyridinium Salts Enabled by NN_2 Pincer Ligand. *Nat. Commun.* **2021**, *12*, 4904. https://doi.org/10.1038/s41467-021-25222-1.
51. Zhu, F.; Li, C.X.; Wu, Z.L.; Cai, T.; Wen, W.; Guo, Q.X. Chiral Aldehyde-Nickel Dual Catalysis Enables Asymmetric α-propargylation of Amino Acids and Stereodivergent Synthesis of NP25302. *Nat. Commun.* **2022**, *13*, 7290. https://doi.org/10.1038/s41467-022-35062-2.
52. Malyshev, D.A.; Scott, N.M.; Marion, N.; Stevens, E.D.; Ananikov, V.P.; Beletskaya, I.P.; Nolan, S.P. Homogeneous Nickel Catalysts for the Selective Transfer of a Single Arylthio Group in the Catalytic Hydrothiolation of Alkynes. *Organometallics* **2006**, *25*, 4462–4470. https://doi.org/10.1021/om060302v.
53. Ananikov, V.P. Nickel: The "Spirited Horse" of Transition Metal Catalysis. *ACS Catal.* **2015**, *5*, 1964–1971. https://doi.org/10.1021/acscatal.5b00072.
54. Brown, D.A.; Glass, W.K.; Fitzpatrick, N.J.; Kemp, T.J.; Errington, W.; Müller-Bunz, H.; Hussein, A.J.; Nimir, H. Mononuclear and Dinuclear Model Hydrolases of Nickel and Cobalt. *Inorg. Chim. Acta* **2005**, *358*, 2755–2762. https://doi.org/10.1016/j.ica.2005.01.029.
55. Routaray, A.; Mantri, S.; Nath, N.; Sutar, A.K.; Maharana, T. Nickel(II) Complex Catalyzed Ring-Opening Polymerization of Lactide. *Polyhedron* **2016**, *119*, 335–341. https://doi.org/10.1016/j.poly.2016.08.032.
56. Sun, J.; Shi, W.; Chen, D.; Liang, C. The Ring-Opening Polymerization Of D,L-Lactide Catalyzed by New Complexes of Cu, Zn, Co, and Ni Schiff Base Derived from Salicylidene And *L*-Aspartic Acid. *J. Appl. Polym. Sci.* **2002**, *86*, 3312–3315. https://doi.org/10.1002/app.11234.
57. Ding, L.; Jin, W.; Chu, Z.; Chen, L.; Lü, X.; Yuan, G.; Song, J.; Fan, D.; Bao, F. Bulk Solvent-Free Melt Ring-Opening Polymerization (ROP) of L-Lactide Catalyzed by Ni(II) and Ni(II)–Ln(III) Complexes Based on the Acyclic Salen-Type Schiff-Base Ligand. *Inorg. Chem. Commun.* **2011**, *14*, 1274–1278. https://doi.org/10.1016/j.inoche.2011.04.040.
58. Xiao, G.; Yan, B.; Ma, R.; Jin, W.J.; Lü, X.Q.; Ding, L.Q.; Zeng, C.; Chen, L.L.; Bao, F. Bulk Ring-Opening Polymerization (ROP) of L-Lactide Catalyzed by Ni(II) and Ni(II)-Sm(II) Complexes Based on a Salen-Type Schiff-Base Ligand. *Polym. Chem.* **2011**, *2*, 659–664. https://doi.org/10.1039/C0PY00385A.
59. Bette, S.; Rincke, C.; Dinnebier, R.E.; Voigt, W. Crystal Structure and Hydrate Water Content of Synthetic Hellyerite, $NiCO_3{\cdot}5.5H_2O$. *Z. Anorg. Allg. Chem.* **2016**, *642*, 652–659. https://doi.org/10.1002/zaac.201600044.
60. Blinou, D.O.; Nikiforov, A.A.; Gurzhiy, V.V.; Minkovich, A.E.; Maksimov, M.Y.; Panina, N.S.; Belyaev, A.N.; Eremin, A.V. Complexes $[Ni_2(\mu\text{-}OH_2)(\mu\text{-}O_2CCH(CH_3)_2)_2L_{2\text{-}4}((CH_3)_2CHCO_2)_2]$: Synthesis, Structure, and Mass Spectrometric Studies. *Russ. J. Coord. Chem.* **2020**, *46*, 81–88. https://doi.org/10.1134/S1070328420020037.
61. Ahlgrén, M.; Turpeinen, U. The Structure of μ-Aqua-Bis(μ-Trifluoroacetato-*O*,*O'*)-Bis[(*N*,*N*,*N'*, *N'*-Tetramethylethylenediamine)(Trifluoroacetato)Nickel(II)]. *Acta Crystallogr. B* **1982**, *38*, 276–279. https://doi.org/10.1107/s0567740882002611.
62. Brown, D.A.; Glass, W.K.; Fitzpatrick, N.J.; Kemp, T.J.; Errington, W.; Clarkson, G.J.; Haase, W.; Karsten, F.; Mahdy, A.H. Structural Variations in Dinuclear Model Hydrolases and Hydroxamate Inhibitor Models: Synthetic, Spectroscopic and Structural Studies. *Inorg. Chim. Acta* **2004**, *357*, 1411–1436. https://doi.org/10.1016/j.ica.2003.08.021.

63. Romakh, V.B.; Therrien, B.; Labat, G.; Stoekli-Evans, H.; Shul'pin, G.B.; Süss-Fink, G. Dinuclear Iron, Ruthenium and Cobalt Complexes Containing 1,4-Dimethyl-1,4,7-Triazacyclononane Ligands as Well as Carboxylato and Oxo or Hydroxo Bridges. *Inorg. Chim. Acta* **2006**, *359*, 3297–3305. https://doi.org/10.1016/j.ica.2006.03.022.
64. Hagen, K.S.; Lachicotte, R.; Kitaygorodskiy, A. Supramolecular Control of Stepwise and Selective Carboxylate Ligand Substitution in Aqua-Carboxylato-Bridged Dimetal(II) Complexes. *J. Am. Chem. Soc.* **1993**, *115*, 12617–12618. https://doi.org/10.1021/ja00079a064.
65. Singh, S.; Saini, D.; Mehta, S.K.; Choquesillo-Lazarte, D. Synthesis, Spectroscopic, and Thermal Analyses of Binuclear Mixed Ligand Co(II) and Ni(II) Complexes. *J. Coord. Chem.* **2011**, *64*, 1544–1553. https://doi.org/10.1080/00958972.2011.575133.
66. Müller, K.; Korb, M.; Koo, C.; Klingeler, R.; Miesel, D.; Hildebrandt, A.; Rüffer, T.; Lang, H. Tri- (M = Cu^{II}) and Hexanuclear (M = Ni^{II}, Co^{II}) Heterometallic Coordination Compounds with Ferrocene Monocarboxylate Ligands: Solid-State Structures and Thermogravimetric, Electrochemical and Magnetic Properties. *Polyhedron* **2017**, *138*, 185–193. https://doi.org/10.1016/j.poly.2017.09.021.
67. Steed, J.W.; Atwood, J.L. *Supramolecular Chemistry*; John Wiley & Sons, Ltd.: Chichester, UK, 2009; p. 990. https://doi.org/10.1002/9780470740880.
68. Dance, I. Distance Criteria for Crystal Packing Analysis of Supramolecular Motifs. *New J. Chem.* **2003**, *27*, 22–27. https://doi.org/10.1039/b206867b.
69. Nikiforov, A.A.; Dubrov, E.N.; Blinou, D.O.; Gurzhiy, V.V.; Selyutin, A.A.; Klyukin, I.N.; Zhdanov, A.P.; Minkovich, A.E.; Panina, N.S.; Eremin, A.V. Penta- and Dinuclear Carboxylate Nickel(II) Complexes with Pyrazole-Based Ligands: Syntheses, Magnetic Properties and DFT Calculations. *Polyhedron* **2021**, *195*, 114971. https://doi.org/10.1016/j.poly.2020.114971.
70. Basolo, F.; Pearson, R.G. *Mechanisms of Inorganic Reactions*, 2nd ed.; John Wiley and Sons, Inc.: New York, NY, USA, 1958; p. 426.
71. Rothenberg, G. *Catalysis: Concepts and Green Applications*; Wiley-VCH: Weinheim, Germany, 2008; p. 279.
72. Chen, Y.-J.; Fang, H.-J.; Hsu, S.C.N.; Jheng, N.-Y.; Chang, H.-C.; Ou, S.-W.; Peng, W.-T.; Lai, Y.-C.; Chen, J.-Y.; Chen, P.-L.; et al. Improving the Ring-Opening Polymerization of ε-Caprolactone and *L*-Lactide Using Stannous Octanoate. *Polym. Bull.* **2013**, *70*, 993–1001. https://doi.org/10.1007/s00289-012-0864-1.
73. Stridsberg, K.M.; Ryner, M.; Albertsson, A.C. Controlled Ring-Opening Polymerization: Polymers with Designed Macromolecular Architecture. *Adv. Polym. Sci.* **2002**, *157*, 41–65. https://doi.org/10.1007/3-540-45734-8_2.
74. Yu, Y.; Fischer, E.J.; Storti, G.; Morbidelli, M. Modeling of Molecular Weight Distribution in Ring-Opening Polymerization of *L*,*L*-Lactide. *Ind. Eng. Chem. Res.* **2014**, *53*, 7333–7342. https://doi.org/10.1021/ie4028999.
75. Coudane, J.; Ustariz-Peyret, C.; Schwach, G.; Vert, M. More about the Stereodependence of DD and LL Pair Linkages during the Ring-Opening Polymerization of Racemic Lactide. *J. Polym. Sci. A Polym. Chem.* **1997**, *35*, 1651–1658. https://doi.org/10.1002/(SICI)1099-0518(19970715)35:9<1651::AID-POLA6>3.0.CO;2-U.
76. Yu, M.; Petrick, L. Untargeted High-Resolution Paired Mass Distance Data Mining for Retrieving General Chemical Relationships. *Commun. Chem.* **2020**, *3*, 157. https://doi.org/10.1038/s42004-020-00403-z.
77. Brine, G.A.; Boldt, K.G.; Prakash, D.; Kotchmar, D.J.; Bondeson, V.C.; Bradley, D.J.; Singh, P.; Carroll, F.I. *P*-Hydroxymethadone: Synthesis, Crystal Structure and CD Properties. *J. Chem. Soc. Perkin Trans. 1* **1991**, 1809–1814. https://doi.org/10.1039/p19910001809.
78. Verkuijl, B.J.V.; Maas, J.C.H. Method for the Manufacture of N,N-diallkyllactamide. U.S. Patent 10,144,702, 7 April 2016.
79. Mostovaya, O.A.; Padnya, P.L.; Shurpik, D.N.; Shiabiev, I.E.; Stoikov, I.I. Novel Lactide Derivatives of *P*-*tert*-Butylthiacalix[4]Arene: Directed Synthesis and Molecular Recognition of Catecholamines. *J. Mol. Liq.* **2021**, *327*, 114806. https://doi.org/10.1016/j.molliq.2020.114806.
80. Alba, A.; du Boullay, O.T.; Martin-Vaca, B.; Bourissou, D. Direct Ring-Opening of Lactide with Amines: Application to the Organo-Catalyzed Preparation of Amide End-Capped PLA and to the Removal of Residual Lactide from PLA Samples. *Polym. Chem.* **2015**, *6*, 989–997. https://doi.org/10.1039/c4py00973h.
81. May, M.; Bardos, T.J.; Barger, F.L.; Lansford, M.; Ravel, J.M.; Sutherland, G.L.; Shive, W. Synthetic and Degradative Investigations of the Structure of Folinic Acid-SF. *J. Am. Chem. Soc.* **1951**, *73*, 3067–3075. https://doi.org/10.1021/ja01151a028.
82. Ogawa, T.; Tomisawa, K.; Sota, K. Preparation of D-Penicillamine. Reaction of Penilloic Acid, Penicilloic Acid α-Amides and Benzylpenicillin with *N*,*N*′-Diphenylethylenediamine. *Heterocycles* **1988**, *27*, 2815–2823. https://doi.org/10.3987/COM-88-4651.
83. Zienty, F.B. Cyclic Thioureas. *J. Am. Chem. Soc.* **1946**, *68*, 1388–1389. https://doi.org/10.1021/ja01211a509.
84. Teng, L.; Xu, X.; Nie, W.; Zhou, Y.; Song, L.; Chen, P. Synthesis and Degradability of a Star-Shaped Polylactide Based on *L*-Lactide and Xylitol. *J. Polym. Res.* **2015**, *22*, 83. https://doi.org/10.1007/s10965-015-0719-1.
85. Wang, B.; Wei, Y.; Li, Z.J.; Pan, L.; Li, Y.S. From $Zn(C_6F_5)_2$ to $ZnEt_2$-Based Lewis Pairs: Significantly Improved Catalytic Activity and Monomer Adaptability for the Ring-Opening Polymerization of Lactones. *ChemCatChem* **2018**, *10*, 5287–5296. https://doi.org/10.1002/cctc.201801488.
86. Sattayanon, C.; Sontising, W.; Limwanich, W.; Meepowpan, P.; Punyodom, W.; Kungwan, N. Effects of Alkoxide Alteration on the Ring-Opening Polymerization of ε-Caprolactone Initiated by *n*-Bu_3SnOR: A DFT Study. *Struct. Chem.* **2015**, *26*, 695–703. https://doi.org/10.1007/s11224-014-0527-y.
87. Trygubenko, S.A.; Wales, D.J. A Doubly Nudged Elastic Band Method for Finding Transition States. *J. Chem. Phys.* **2004**, *120*, 2082–2094. https://doi.org/10.1063/1.1636455.

88. Ryner, M.; Stridsberg, K.; Albertsson, A.C.; von Schenck, H.; Svensson, M. Mechanism of Ring-Opening Polymerization of 1,5-Dioxepan-2-One and *L*-Lactide with Stannous 2-Ethylhexanoate. A Theoretical Study. *Macromolecules* **2001**, *34*, 3877–3881. https://doi.org/10.1021/ma002096n.
89. Lin, Y.F.; Jheng, N.Y. Mechanistic Insight into the Ring-Opening Polymerization of ε-Caprolactone and *L*-Lactide Using Ketiminate-Ligated Aluminum Catalysts. *Polymers* **2019**, *11*, 1530. https://doi.org/10.3390/polym11091530.
90. Nifant'ev, I.; Ivchenko, P. Coordination Ring-Opening Polymerization of Cyclic Esters: A Critical Overview of DFT Modeling and Visualization of the Reaction Mechanisms. *Molecules* **2019**, *24*, 4117. https://doi.org/10.3390/molecules24224117.
91. Báthori, N.B.; Nassimbeni, L.R. Selectivity of Amides by Host-Guest Inclusion. *CrystEngComm* **2011**, *13*, 3156–3161. https://doi.org/10.1039/c0ce00362j.
92. Morozov, I.V.; Karpova, E.V.; Glazunova, T.Y.; Boltalin, A.I.; Zakharov, M.A.; Tereshchenko, D.S.; Fedorova, A.A.; Troyanov, S.I. Trifluoroacetate Complexes of 3d Elements: Specific Features of Syntheses and Structures. *Russ. J. Coord. Chem.* **2016**, *42*, 647–661. https://doi.org/10.1134/S107032841610002X.
93. Chaboussant, G.; Basler, R.; Güdel, H.U.; Ochsenbein, S.; Parkin, A.; Parsons, S.; Rajaraman, G.; Sieber, A.; Smith, A.A.; Timco, G.A.; et al. Nickel Pivalate Complexes: Structural Variations and Magnetic Susceptibility and Inelastic Neutron Scattering Studies. *Dalton Trans.* **2004**, 2758–2766. https://doi.org/10.1039/b406112h.
94. Spackman, M.A.; Jayatilaka, D. Hirshfeld Surface Analysis. *CrystEngComm* **2009**, *11*, 19–32. https://doi.org/10.1039/b818330a.
95. Turner, M.J.; McKinnon, J.J.; Wolff, S.K.; Grimwood, D.J.; Spackman, P.R.; Jayatilaka, D.; Spackman, M.A. *CrystalExplorer17*; The University of Western Australia: Perth, Australia, 2017.
96. CrysAlisPro. *Rigaku Oxford Diffraction*, Version 1.171.36.32.; Rigaku: Tokyo, Japan, 2013.
97. Sheldrick, G.M. *SHELXT*—Integrated Space-Group and Crystal-Structure Determination. *Acta Crystallogr. A Found. Adv.* **2015**, *A71*, 3–8. https://doi.org/10.1107/S2053273314026370.
98. Sheldrick, G.M. Crystal Structure Refinement with *SHELXL*. *Acta Crystallogr. C Struct. Chem.* **2015**, *C71*, 3–8. https://doi.org/10.1107/S2053229614024218.
99. Dolomanov, O.V.; Bourhis, L.J.; Gildea, R.J.; Howard, J.A.K.; Puschmann, H. *OLEX2*: A Complete Structure Solution, Refinement and Analysis Program. *J. Appl. Crystallogr.* **2009**, *42*, 339–341. https://doi.org/10.1107/S0021889808042726.
100. Spek, A.L. PLATON SQUEEZE: A Tool for the Calculation of the Disordered Solvent Contribution to the Calculated Structure Factors. *Acta Crystallogr. C Struct. Chem.* **2015**, *C71*, 9–18. https://doi.org/10.1107/S2053229614024929.
101. Neese, F. Software Update: The ORCA Program System, Version 4.0. *Wiley Interdiscip. Rev. Comput. Mol. Sci.* **2018**, *8*, e1327. https://doi.org/10.1002/wcms.1327.
102. Neese, F.; Wennmohs, F.; Becker, U.; Riplinger, C. The ORCA Quantum Chemistry Program Package. *J. Chem. Phys.* **2020**, *152*, 224108. https://doi.org/10.1063/5.0004608.
103. Adamo, C.; Barone, V. Toward Reliable Density Functional Methods without Adjustable Parameters: The PBE0 Model. *J. Chem. Phys.* **1999**, *110*, 6158. https://doi.org/10.1063/1.478522.
104. Brandenburg, J.G.; Bannwarth, C.; Hansen, A.; Grimme, S. B97-3c: A Revised Low-Cost Variant of the B97-D Density Functional Method. *J. Chem. Phys.* **2018**, *148*, 064108. https://doi.org/10.1063/1.5012601.
105. Weigend, F.; Ahlrichs, R. Balanced Basis Sets of Split Valence, Triple Zeta Valence and Quadruple Zeta Valence Quality for H to Rn: Design and Assessment of Accuracy. *Phys. Chem. Chem. Phys.* **2005**, *7*, 3297–3305. https://doi.org/10.1039/b508541a.
106. Panina, N.S.; Nikiforov, A.A.; Blinou, D.O.; Dubrov, E.N.; Ponyaev, A.I.; Eremin, A.V.; Belyaev, A.N. Formation of Oligo-Nuclear Carboxylate Nickel(II) Complexes with Nitrogen-Containing Ligands. Quantum-Chemical Simulation. *Russ. J. Gen. Chem.* **2019**, *89*, 2264–2272. https://doi.org/10.1134/S1070363219110173.
107. Henkelman, G.; Jónsson, H. Improved Tangent Estimate in the Nudged Elastic Band Method for Finding Minimum Energy Paths and Saddle Points. *J. Chem. Phys.* **2000**, *113*, 9978. https://doi.org/10.1063/1.1323224.
108. Henkelman, G.; Arnaldsson, A.; Jónsson, H. Theoretical Calculations of CH_4 and H_2 Associative Desorption from Ni(111): Could Subsurface Hydrogen Play an Important Role? *J. Chem. Phys.* **2006**, *124*, 044706. https://doi.org/10.1063/1.2161193.
109. Mills, G.; Jónsson, H.; Schenter, G.K. Reversible Work Transition State Theory: Application to Dissociative Adsorption of Hydrogen. *Surf. Sci.* **1995**, *324*, 305–337. https://doi.org/10.1016/0039-6028(94)00731-4.